



HAL
open science

Deciphering recycling processes during solar system evolution from magnesium-rich relict olivine grains in type II chondrules

Gabriel A Pinto, Emmanuel Jacquet, Alexandre Corgne, Felipe Olivares, Johan Villeneuve, Yves Marrocchi

► **To cite this version:**

Gabriel A Pinto, Emmanuel Jacquet, Alexandre Corgne, Felipe Olivares, Johan Villeneuve, et al.. Deciphering recycling processes during solar system evolution from magnesium-rich relict olivine grains in type II chondrules. *Geochimica et Cosmochimica Acta*, 2024, 364, pp.65 - 78. 10.1016/j.gca.2023.11.012 . hal-04636884

HAL Id: hal-04636884

<https://hal.science/hal-04636884>

Submitted on 5 Jul 2024

HAL is a multi-disciplinary open access archive for the deposit and dissemination of scientific research documents, whether they are published or not. The documents may come from teaching and research institutions in France or abroad, or from public or private research centers.

L'archive ouverte pluridisciplinaire **HAL**, est destinée au dépôt et à la diffusion de documents scientifiques de niveau recherche, publiés ou non, émanant des établissements d'enseignement et de recherche français ou étrangers, des laboratoires publics ou privés.

1 **Deciphering recycling processes during solar system evolution**
2 **from Mg-rich relict olivine grains in type II chondrules**

3
4 Gabriel A. Pinto^{1,2}, Emmanuel Jacquet³, Alexandre Corgne⁴, Felipe Olivares²,
5 Johan Villeneuve¹ & Yves Marrocchi^{1,*}

6
7
8 ¹Université de Lorraine, CNRS, CRPG, UMR 7358, Vandœuvre-lès-Nancy, 54501, France

9 ²INCT, Universidad de Atacama, Copayapu 485, Copiapó, Chile

10 ³Institut de Minéralogie, de Physique des Matériaux et de Cosmochimie (IMPMC), Muséum
11 national d'Histoire naturelle, Sorbonne Université, CNRS, CP52, 57 rue Cuvier, 75005 Paris,
12 France.

13 ⁴Instituto de Ciencias de la Tierra, Universidad Austral de Chile, Valdivia, Chile

14
15 *Corresponding author: yvesm@crpg.cnrs-nancy.fr

16
17 **Abstract**

18 Ferromagnesian chondrules present a remarkable dichotomy between reduced (type I)
19 and oxidized (type II) varieties. How these formed, and how they may be related remains
20 contentious. Many type II chondrules, especially in carbonaceous chondrites, contain
21 forsteritic grains in disequilibrium with FeO-rich host olivine grains, which must be relicts of
22 precursor material. In this study, we analyzed the oxygen isotopic composition of magnesian
23 relict and host olivine grains in type II chondrules in CO and CR chondrites. The analyzed
24 relicts are generally more ¹⁶O-rich than host grains and plot in the range (isotopic and mineral
25 chemical) of type I chondrules in carbonaceous chondrites. Remarkably, they tend to cluster
26 around the dominant $\Delta^{17}\text{O}$ peaks of the type I chondrules in their host chondrites, viz. -6‰
27 and -2‰ for CO and CR, respectively. With the occurrence of relatively intact type I
28 chondrules within some type II chondrules, this corroborates that local type I chondrules were
29 among the precursors of type II chondrules, and that chondrule formation occurred within the
30 accretion reservoir of the eventual chondrites. This supports the nebular brand of chondrule-
31

32 forming scenarios. Since not all previous generations of chondrules (or other precursor
33 objects) have been recycled, chondrule formation events must also have been extremely
34 localized.

35
36

37 **Keywords**

38 Carbonaceous chondrites, chondrules, oxygen isotopes, recycling processes, protoplanetary
39 disk

40

41

42

43

44

45

46

47

48

49

50

51

52

53

54

55

56

57

58

59

60

61

62

63

64

65

66

67

68
69
70
71
72
73

1- Introduction

74 The evolution of the circumsolar disk led to the formation of solids through a wide
75 range of processes such as evaporation/condensation (Ebel et al., 2018; Marrocchi et al.,
76 2019a), fusion/crystallization (Connolly & Jones, 2016) and thermal annealing (Han &
77 Brearley, 2015). The resulting dust provided the various building blocks of asteroids and
78 planets, either in the form of refractory inclusions (i.e., CAIs = Calcium Aluminum-rich
79 Inclusions and AOA = Amoeboid Olivine Aggregates), chondrules and fine-grained matrix.
80 The mineralogical, petrographic, and isotopic features of these early solids thus represent a
81 powerful proxy for deciphering the conditions that prevailed in the circumsolar disk and how
82 they evolved with time.

83 The mm-sized igneous spheroids called chondrules are the most abundant high-
84 temperature components of both non-carbonaceous (NC) and carbonaceous (C) chondrites,
85 which most likely represent material from the inner and outer solar system, respectively
86 (Kruijer et al., 2017; Schneider et al., 2020). This suggests that the whole circumsolar disk
87 was affected by chondrule production and/or redistribution. The most abundant chondrules
88 are ferromagnesian porphyritic chondrules that can be classified to first order into type I and
89 type II chondrules, depending on their oxidation state (Jones, 2012). Type I chondrules are
90 more reduced than type II chondrules. This translates into high and low Mg# ($\equiv 100 \times$ molar
91 ratio $\text{Mg}/(\text{Mg}+\text{Fe})$) for type I and type II chondrules, respectively. While the limit between
92 type I and type II is arbitrarily defined as $\text{Mg}\# = 90$, there is a hiatus between the two types,
93 with few chondrules between Mg# of 90 and 97 (e.g., Villeneuve et al., 2015). Type II
94 chondrules are predominantly observed in ordinary chondrites but are consistently present in
95 all types of carbonaceous chondrites (Jones, 2012).

95 Type I chondrules are complex objects whose mineralogy, textures, and chemical and
96 isotopic compositions result from multi-step processes involving precursor recycling, melting
97 event(s) and complex gas-melt interactions (Ebel et al., 2018; Libourel & Portail, 2018;
98 Marrocchi et al., 2018, 2019b; Schneider et al., 2020; Tenner et al., 2018; Villeneuve et al.,
99 2020). The mechanism(s) at their origin remain(s) however controversial: they may
100 correspond to melted aggregates of nebular dust (Hewins et al., 2005; Piralla et al., 2021), e.g.
101 because of bow shocks induced by eccentric planetary embryos (Morris et al., 2012), or by-
102 products of planetary collisions (Johnson et al., 2015; Libourel et al., 2022; Libourel & Krot,
103 2007). In addition, type I chondrule formation took place over a long period of time (i.e., 3–4
104 Ma; (Bollard et al., 2017; Piralla et al., 2023) and could have been repeated, as supported by
105 evidence for distinct generations of chondrules in CR chondrites (Marrocchi et al., 2022).
106 Compared to reduced and volatile-depleted type I chondrules, type II chondrules are
107 characterized by FeO-rich silicates and more chondritic abundances of moderately volatile
108 elements (e.g., Jacquet et al., 2015). The more oxidized conditions of type II chondrule
109 formation could result from either formation in regions with higher dust to gas ratios
110 (Schrader et al., 2013) or lower carbon content in the precursors (Connolly et al., 1994). It has
111 been also proposed that type II chondrules derived from their type I counterparts through
112 nebular oxidation shocks (Villeneuve et al., 2020) or within impact-generated vapor plumes
113 (Libourel et al., 2023).

114 Oxygen isotopes may provide more constraints into the formation conditions of both
115 type I and type II chondrules and their potential relationship. First, chondrule isotopic
116 compositions are widely separated from those of AOAs and CAIs (very ^{16}O -rich, with $\Delta^{17}\text{O} =$
117 $\delta^{17}\text{O} - 0.52 \times \delta^{18}\text{O}$ around -25 ‰; e.g., (Krot et al., 2004). There is also a systematic
118 difference between type I and type II chondrules, especially in carbonaceous chondrites,
119 where the former are ^{16}O -richer than the latter (Libourel et al., 2023; Schrader et al., 2013;

120 Tenner et al., 2018; Ushikubo & Kimura, 2020). Likewise, there are some differences
121 depending on the reservoir of origin with type I chondrules in (i) CO–CM–CV chondrites
122 having $\Delta^{17}\text{O}$ ranging from -7 to -4 ‰ with a maximum observed near -6 ‰ (Tenner et al.,
123 2018; Ushikubo and Kimura, 2020) and (ii) CR chondrules that are characterized by $\Delta^{17}\text{O}$
124 varying from -6 to -1 ‰ and peaking circa -2 ‰ (Marrocchi et al., 2022; Schrader et al.,
125 2014; Tenner et al., 2015). The recent characterization of the chemical and isotopic
126 compositions of relict olivine grains in different carbonaceous chondrites suggest that type I
127 chondrules derived (in part) from AOA-like precursors (Marrocchi et al., 2018, 2019b), in
128 agreement with (i) trace element signatures ((Jacquet, 2021; Jacquet & Marrocchi, 2017;
129 Ruzicka et al., 2007) and (ii) ^{50}Ti and ^{54}Cr excesses (Schneider et al., 2020).

130 ^{16}O -rich forsteritic olivine grains have been occasionally reported in type II chondrules
131 ((Jones, 1996, 2012; Kunihiro et al., 2004, 2005; Libourel et al., 2023; Schrader et al., 2015,
132 2018; Wasson & Rubin, 2003; Yurimoto & Wasson, 2002). The similitude of such grains
133 with type I chondrules in the same chondrites have long suggested that these were relicts of
134 type I chondrules, hence highlighting a potential link between type I and type II chondrules.
135 This was also proposed based on the similar large silicon isotopic variations observed within
136 type I chondrules and in Mg-rich olivine relict grains in type II chondrules (Villeneuve et al.,
137 2020). However, no systematic chemical and oxygen isotopic characterization of Mg-rich
138 relict olivine grains in type II chondrules has been performed. In this study, we report a
139 comprehensive survey of the oxygen isotopic compositions of relict-bearing type II
140 chondrules in carbonaceous chondrites, where they are proportionally most abundant,
141 specifically in CO and CR chondrites. We use our data to quantify the conditions of formation
142 of type II chondrules and discuss the implications for the reprocessing of primordial dust in
143 the outer circumsolar disk.

144

145

146

147 **2- Material and Methods**

148

149 We surveyed all chondrules within (i) four home-made thick sections of CO3
150 carbonaceous chondrites (Los Vientos 123 [CO3.05], Catalina 008 [CO3.1], El Medano 463
151 and 465 [CO3.2]) and (ii) two thick sections of CR2 carbonaceous chondrites (Renazzo and
152 Dar al Gani 574, sections no. 719sp3 and 3681sp2, respectively; from the Muséum national
153 d'Histoire naturelle, Paris, France). The petrography and mineralogy of type II chondrules
154 were determined by optical microscopy, backscattered electron (BSE) imaging, and X-ray
155 compositional mapping. For the latter two, we used (i) a Zeiss Evo MA10 equipped with an
156 Oxford X-MAX N 20 SDD energy dispersive spectrometer and operating with a 3 nA
157 electron beam accelerated at 15 kV (Universidad de Atacama, Copiapó, Chile) and (ii) a
158 JEOL JSM-6510 scanning electron microscope equipped with a Genesis EDX detector using
159 a 3 nA electron beam accelerated at 15 kV (CRPG-CNRS, Nancy, France).

160 Thirteen type II chondrules with and without apparent Mg-rich relicts were selected: 8
161 in COs and 5 in CRs chondrites. Quantitative analyses of Al, Ti, Ca, Cr, Mn, Ni, Mg, Fe, and
162 Si in all olivine grains large enough to be isotopically characterized by SIMS were performed
163 using a CAMECA SX-Five electron microprobe at the CAMPARIS service (Sorbonne
164 University, Paris, France). The microprobe was calibrated using the following natural and
165 synthetic standards for silicate analyses: diopside (Si, Ca, Mg), orthoclase (Al), MnTiO₃ (Mn,
166 Ti), Cr₂O₃ (Cr), and Fe₂O₃ (Fe). A 20 nA focused beam, accelerated to 15 kV potential
167 difference, was used for spot analyses of olivine with 20 s analysis times. Detection limits in
168 silicates were 0.03 wt% for SiO₂, Al₂O₃, CaO and MgO; 0.04 wt% for MnO and TiO₂, and

169 0.07 wt% for NiO, Cr₂O₃ and FeO. The PAP software was used for matrix corrections
170 (Pouchou and Pichoir, 1984).

171 We measured the oxygen isotopic compositions of olivine grains with varied iron
172 contents in type II chondrules using Secondary Ion Mass Spectrometry (SIMS). We used the
173 CAMECA IMS 1270 E7 at the Centre de Recherches Pétrographiques et Géochimiques
174 (CRPG-CNRS, Nancy, France). ¹⁶O⁻, ¹⁷O⁻, and ¹⁸O⁻ ions produced by a Cs⁺ primary ion
175 beam (~10 μm, ~2–2.5 nA, rastered over 5 × 5 μm²) were measured in multi-collection mode
176 using three Faraday cups (FCs). To remove the interference of ¹⁶OH⁻ on the ¹⁷O⁻ peak and to
177 maximize the flatness atop the ¹⁶O⁻ and ¹⁸O⁻ peaks, the entrance and exit slits of the central
178 FC were adjusted to obtain mass resolution power (MRP = $M/\Delta M$) of ~7,000 for ¹⁷O⁻. As an
179 additional safeguard against ¹⁶OH⁻ interference, a liquid N₂ trap was used to reduce the
180 pressure in the analysis chamber to <1 × 10⁻⁸ mbar. The two off-axis multicollection FCs, L'2
181 and H1, were respectively used to measure ¹⁶O⁻ and ¹⁸O⁻ and were set on exit slit 1 (MRP =
182 2,500). We used 10¹⁰ Ω, 10¹² Ω, and 10¹¹ Ω resistors for the L'2 (¹⁶O), central (¹⁷O), and H1
183 (¹⁸O) FCs, respectively (see Bouden et al. 2021 for further details). A normal-incidence
184 electron gun was used for charge compensation. Total measurement times were 300 s,
185 comprising 120 s of pre-sputtering and 180 s of analysis. Two terrestrial standards, San Carlos
186 olivine and JV1 diopside, were used to define the mass-dependent fractionation line. The
187 instrumental mass fractionation (IMF) and matrix effect of chondrule olivine grains was
188 corrected using San Carlos olivine and a set of synthetic standard olivines with Mg# ranging
189 from 36 to 100 (Villeneuve et al., 2019, 2020). To monitor any instrumental drift and to
190 achieve good precision, the San Carlos olivine was analyzed after every 10–15 sample
191 analyses. Typical count rates obtained on San Carlos olivine were 1.0 × 10⁹ cps, 4.0 × 10⁵ cps,
192 and 2.1 × 10⁶ cps for ¹⁶O, ¹⁷O, and ¹⁸O, respectively. All SIMS analytical spots were checked
193 thoroughly by scanning electron microscopy, and any spot near fractures, in the mesostasis, or

194 not completely within olivine grains was excluded from the dataset. Oxygen isotopic
195 compositions are expressed in δ units as $\delta^{17,18}\text{O} = [({}^{17,18}\text{O}/{}^{16}\text{O})_{\text{sample}}/({}^{17,18}\text{O}/{}^{16}\text{O})_{\text{V-SMOW}} - 1] \times$
196 1000 ‰ where V-SMOW refers to the Vienna Standard Mean Ocean Water value. Samples
197 related by mass-dependent fractionation to the composition of V-SMOW fall on a line with a
198 slope of 0.52 (defining as the Terrestrial Fractionation Line, TFL; Clayton et al., 1991)
199 whereas mass-independent variations are described by $\Delta^{17}\text{O} = \delta^{17}\text{O} - 0.52 \times \delta^{18}\text{O}$
200 (representing vertical deviations from the TFL in a triple oxygen isotope diagram). Typical 2σ
201 measurement errors, accounting for internal errors on each measurement and the external
202 reproducibility of the standards, were estimated to be ~ 0.4 ‰ for $\delta^{18}\text{O}$, ~ 0.7 ‰ for $\delta^{17}\text{O}$, and
203 ~ 0.7 ‰ for $\Delta^{17}\text{O}$.

204

205 **3- Results**

206

207 **3.1- Petrography and chemistry**

208

209 We examined all type II chondrules in the five thick sections and selected 13
210 chondrules with minimum evidence of secondary alteration and olivine grains large enough to
211 perform detailed chemical profiles and isotopic analysis (**Figs. 1–2**). The chondrules are fairly
212 rounded but not, in general, perfectly circular in cross-section, and some may be actually
213 compound (e.g., **Fig. 1c,f** & **Fig. 2c,e**; see also Jacquet 2021). They all display porphyritic
214 texture (except EM463_Ch05, **Fig. 2f**), with several subhedral to euhedral Fe-rich olivine
215 grains immersed in well-preserved glassy mesostases (**Figs. 1–2**). The maximum apparent
216 diameter of chondrules ranges from 250 to 740 μm and 400 to 750 μm in CO and CR
217 chondrites, respectively. Among the 13 type II chondrules, 11 exhibit Mg-Fe zoning with
218 sharply defined Mg-rich cores and abrupt FeO and/or CaO variation in the chemical profiles

219 (Figs. 1–2), similar to the relict-bearing chondrules described by Jones et al., (2018). Some
220 relict-bearing chondrules (e.g., LoV123_Ch02, Fig. 1a) display several forsteritic grains
221 showing Mg diffusion and sharper border inside either larger or smaller Fe-rich olivine grains.
222 The position of relict grains is random, and most of them were found as (i) isolated
223 phenocrysts with Fe-rich rims or (ii) clusters of 3 or (sometimes much) more phenocrysts,
224 where each grain is surrounded by a Fe-rich mantle (Figs. 1–2). Sometimes, the Mg-rich
225 olivine is even part of a more or less intact type I chondrule-like object, with enstatite (stricto
226 sensu, i.e., Fs < 10 mol%), mesostasis and/or metal grains (Fig. 1d & Fig. 2a,b,c), at variance
227 with the contention of Libourel et al. (2023) that enstatite virtually never occurs in type II
228 chondrules. Troilite and chromite are the main opaque and accessory phases in all described
229 FeO-rich chondrules. They are contained in the mesostasis and display sizes up to 90 μm ,
230 except for CR, where troilite reaches up to 200 μm .

231 The mean chemical composition of relict and host olivine grains among the 13
232 chondrules is shown in Table 1. The Mg# of olivine grains varies widely in the selected
233 chondrules, from 24.6 to 98.3 (Table S1), depending on whether the olivine is a host or relict
234 grain. Host olivine grains in CO and CR chondrites display mean Mg# (\pm standard deviation)
235 of 48.9 ± 11.8 (N= 447) and 51.8 ± 6.1 (N= 22), respectively. Previous values estimated in
236 host olivine show somewhat higher Mg# for CO and CR chondrites (~66 and 71, respectively;
237 Berlin et al., 2011), but this may hinge on our relict-centered chondrule selection, biasing
238 against large uniformly host (i.e., relict-free) phenocrysts (with less ferroan cores), thus
239 confining host analyses to (more ferroan) overgrowths of large grains or small phenocrysts.
240 As expected, while showing a large range of Fa values (1.8 to 41.8 mol% in CO), relict
241 olivine grains tend to be more forsteritic, with mean Mg# of 85.0 ± 10.6 (N= 189) and $84.3 \pm$
242 12.9 (N= 15) for CO and CR chondrites. 70 % of relicts in CR chondrules and 38 % of relicts
243 in CO chondrules (Table S2) display Fa values < 10 mol%, that is, in type I compositional

244 territory (**Fig. 2**), but the other obviously exited it only because of diffusion of Fe from the
245 host chondrule.

246 Commonly, Mg-rich relicts in type II chondrules are MnO-poor, and slightly CaO-rich
247 compared to their host olivine grains (**Table 1**). Host olivines display higher mean MnO (0.35
248 and 0.27 wt%, respectively) and Cr₂O₃ (0.42 vs. 0.25 wt%) in CR than CO chondrites,
249 consistent with earlier data (e.g., Berlin et al., 2011; Schrader et al., 2015).

250

251 **3.2- Oxygen Isotopes**

252

253 We performed a total of 88 O-isotopic measurements of relicts and host grains (**Table**
254 **2**); 26 and 62 spots were made in CR and CO chondrites, respectively. The olivine O-isotopic
255 composition in CO and CR chondrites ranges respectively from -13.1 to +15.2 ‰ and -11.3
256 to 8.1 ‰ for $\delta^{18}\text{O}$; and from -14.2 to 5.8 ‰ and -13.1 to 4.4 ‰, in the case of $\delta^{17}\text{O}$. $\Delta^{17}\text{O}$
257 ranges from -7.7 to +0.7 ‰. In the three-oxygen diagram (**Fig. 3a**), our data plot along the
258 PCM line proposed by Ushikubo et al. (2012).

259 Most relict olivine grains are ¹⁶O-rich compared to those in their Fe-rich host
260 phenocrysts (**Figs. 3–4**). However, 36 % (4 over 11) of relict-bearing chondrules show an
261 overlap or similar O-isotopes signature. Only one relict grain in the biggest phenocryst of
262 LoV123_Ch02 (**Fig. 4a**) shows the opposite relation to its host. The mean $\Delta^{17}\text{O}$ values of
263 relict grains in CO and CR chondrites are -4.7 and -2.8 ‰, lower than the mean $\Delta^{17}\text{O}$ values
264 in type II olivine hosts: -2.6 and -0.5 ‰ for CO and CR chondrites, respectively (**Fig. 5**).
265 Analogous difference of the mean $\Delta^{17}\text{O}$ values have been reported between relict and host
266 grains in type I chondrules for CR (-5.2 and -3.4 ‰; Marrocchi et al., 2022). The latest
267 indicate a larger $\Delta^{17}\text{O}$ difference between relict and host grains from type II chondrules (**Figs.**
268 **6–8**). Same was observed by Tenner et al. (2013) for type II chondrules in CO3.0 chondrite

269 Yamato 81020. In our data set, the isotopic compositions do not show any correlation with
270 size or location within chondrules.

271 Host grains tend to be isotopically uniform within each chondrule, but there are three
272 apparent exceptions, LoV098-Ch02p, Ren_Ch01 and DaG574_Ch01 (**Fig. 4**). In the former
273 two, the exception is restricted to one outlying ^{16}O -rich grain ($\Delta^{17}\text{O} = -1.3$ and -3.0 ‰,
274 respectively). In the latter, three Fe-rich “host” grains show three distinct $\Delta^{17}\text{O}$ values (-4.7 , $-$
275 3.0 and 0.5 ‰; **Table S2**). Two of them in the latter, and the former two may be isotopic
276 relicts in the sense of Ushikubo et al. (2012) but no longer recognizable in Mg# because of Fe
277 diffusion.

278 Generally, Mg-rich relicts among CO and CR chondrites overlap the oxygen isotopic
279 composition of relict and host olivine grains in type I chondrules (**Figs 3–4**). In particular, all
280 relicts in CR chondrites plot around -6 ‰ or -2 ‰, i.e. the $\Delta^{17}\text{O}$ values characteristic of the
281 two generations of type I CR chondrules (“type I-CO” and “type I-CR”) described by
282 Marrocchi et al. (2022). The most ^{16}O -rich grain found (in chondrule Ren_Ch03) has a mean
283 $\Delta^{17}\text{O}$ value of -7.5 ± 0.4 ‰. Yet most relicts (8/10 = 80 %) are in type I-CR territory (i.e.,
284 $\Delta^{17}\text{O} > -4$ ‰; Marrocchi et al., 2022), as are most type I chondrules in CR. In contrast, type II
285 chondrule forsteritic relicts in CO chondrites are mostly in type I-CO territory (i.e., $\Delta^{17}\text{O} < -4$
286 ‰), as are most type I chondrules there (e.g., Tenner et al., 2013; Libourel et al., 2023).

287

288 **4- Discussion**

289

290 **4.1- The source of Mg-rich relict grains in type II chondrules**

291

292 Although type II chondrules have been less studied than their type I counterparts, their
293 formation conditions are no less controversial. They have been historically interpreted as

294 resulting from closed-system, fractionally crystallized droplets heated at near-liquidus
295 temperature and cooled at $\sim 1\text{--}500$ K/h (see Jones et al., 2018 for a review). The larger size of
296 type II chondrules and their higher concentrations of volatile and moderately volatile elements
297 (i.e., Na, K, Mn, Cr, S, and Fe) compared to type I chondrule were used as arguments for
298 suggesting formation in different nebular (sub)-reservoir than type I chondrules (Hewins &
299 Zanda, 2012; Jacquet et al., 2015). Comprehensive oxygen isotopic observations also suggest
300 the formation of type I and type II chondrules in environments characterized by distinct
301 dust/gas ratios and water ice enhancement, type II being formed in location with dust-
302 enrichment factors up to ~ 4000 above solar (Chaumard et al., 2018, 2021; Hertwig et al.,
303 2018; Tenner et al., 2015). This suggested that type I and type II chondrules formed in two
304 different astrophysical settings, possibly on different sides of the snowline (Tenner et al.,
305 2018). However, the common presence of Mg-rich relict olivine grains within type II
306 chondrules (**Figs. 1–2**) as well as their chemical and isotopic features (**Figs. 3–8**) suggest that
307 type II chondrules derive from type I chondrules through oxidation shocks¹ and protracted
308 gas-melt interactions (Ruzicka et al., 2008, Schrader et al., 2015, 2018; Ebel et al., 2018;
309 Villeneuve et al., 2020). A comprehensive experimental approach also showed that these
310 processes can account for several prominent features of type II chondrules, such as chemical
311 zoning in olivine grains and the preservation of Mg-rich olivine relict grains (Villeneuve et
312 al., 2015).

313 Most of our Mg-rich relict olivine grains in type II chondrules are ^{16}O -rich compared
314 to their Fe-rich host phenocrysts (**Figs 3–4**). Mg-rich relict grains with $\Delta^{17}\text{O}$ values < -15 ‰
315 were also reported in type II chondrules from CO and CV chondrites (Jones et al., 2002;
316 Libourel et al., 2023; Yurimoto & Wasson, 2002), thus advising a possible genetic link with
317 refractory inclusions (Krot, 2019). However, all our relict grains in CO chondrites display

¹ The expression "oxidation shock" should not be construed to imply a shock wave chondrule-forming scenario.

318 $\Delta^{17}\text{O}$ values ranging from -7.7 to -0.1 ‰ ($n = 8$), similar to those reported in the pristine
319 CO3.05 Yamato 81020 (-11.4 ‰ $< \Delta^{17}\text{O} < 0.2$ ‰, $n = 11$; Kunihiro et al., 2004; Tenner et al.,
320 2013). Lumping this with previous literature data, this indicates that only ~ 11 % (3 out of 27)
321 of relicts sample ^{16}O -rich dust similar to refractory inclusions (this study; Yurimoto and
322 Wasson, 2002; Kunihiro et al., 2004; Tenner et al., 2013; Libourel et al., 2023).

323 Mg-rich relicts in type II chondrules always plot in the range of O-isotopic
324 composition of host olivines in type I chondrules (**Figs. 4–6**), and mostly near the dominant
325 mode for type I chondrules in the same chondrites (i.e., near $\Delta^{17}\text{O} = -6$ ‰ in CO and $\Delta^{17}\text{O} =$
326 -2 ‰ in CR; **Figs 4–6**). Some outlying Fe-rich “host” grains also do as well (for the CR
327 chondrules Ren_Ch01 and DaG574_Ch01, **Fig. 4i,l**) and may have been of the same nature,
328 but their Mg# was likely overprinted by Fe diffusion during chondrule melting. The mineral
329 chemistry of Mg-rich grains in type II chondrules is also similar to type I chondrule olivine,
330 not only in terms of Fa content, but also in minor element content, e.g. depletion in MnO and
331 enrichment in CaO (**Figs 5–8**). We also observe varying degrees of assimilation of type I
332 chondrules in type II hosts, from relicts corresponding to whole type I chondrules to more or
333 less identifiable forsterite clusters (**Figs 1–2**). This suggests that Mg-relicts in type II
334 chondrules originate mainly from Mg-rich type I chondrules, pointing toward a genetic link
335 between both types of chondrules with type II being derived from type I chondrules *via*
336 oxidation shocks inducing the dissolution of Fe-Ni metal beads and the subsequent
337 crystallization of FeO-rich olivine overgrowths (Ruzicka et al., 2008; Schrader et al., 2015,
338 2018; Villeneuve et al., 2015, 2020; Libourel et al., 2023).

339

340 **4.2 Implications for chondrule formation**

341

342 Establishing a genetic relationship between type I and type II chondrules does not in
343 itself provide any information on their environments of formation, as both nebular and
344 planetary conditions may be invoked (e.g., Tenner et al., 2015; Libourel et al., 2023). Libourel
345 et al., (2023) recently proposed that both types of chondrules formed within an isotopically
346 heterogeneous impact-generated vapor plume with a type I-CO-like core region (i.e., $\Delta^{17}\text{O} < -$
347 4 ‰) gradually mixing with type I-CR surroundings (i.e., $\Delta^{17}\text{O} > -4 \text{ ‰}$). In such a
348 framework (the impact splash scenario; e.g., Sanders & Scott, 2012; or the jetting scenario;
349 Johnson et al. 2015), type II chondrules derive from first-formed type I chondrules following
350 the drop in the vapor plume temperature (in its outer regions) under unbuffered redox
351 conditions (Libourel et al., 2023). However, several observations weaken this interpretation
352 and, in contrast, favor evolving nebular settings and episodic recycling:

353 1– Type I chondrules in carbonaceous chondrites commonly display relict grains with
354 chemical (Al-Ti-poor) and isotopic ($\Delta^{17}\text{O} < -15 \text{ ‰}$) similar to olivine grains present within
355 AOAs (**Fig. 9**; Marrocchi et al., 2018, 2019b; Schneider et al., 2020; Jacquet et al., 2021). In
356 addition, isolated type I chondrules from carbonaceous chondrites show variable ^{50}Ti and ^{54}Cr
357 nucleosynthetic anomalies, most of which differing from the host chondrite compositions
358 (Schneider et al., 2020). These isotopic variations suggest that type I CC chondrules were
359 partially formed from precursors isotopically similar to ^{50}Ti - ^{54}Cr -rich CAIs and AOAs
360 (Gerber et al., 2017; Schneider et al., 2020; Burkhardt et al., 2023). This thus appears difficult
361 to reconcile with the impact scenario as it would imply that nearly each melt droplet from the
362 impact plume ingested unmelted and unvaporized refractory inclusions wandering in the
363 impact vapor plume.

364 2– The correlation between Mg# and $\Delta^{17}\text{O}$ reported in the literature (e.g., Tenner et
365 al., 2018 and references therein; Kita et al., 2022) for type I chondrules supports
366 systematically different oxygen fugacities in the type I-CO and type I-CR isotopic reservoirs

367 (e.g., Schrader et al., 2013; Tenner et al., 2015), or different cooling rates (Jacquet et al.,
368 2021) and hence their likely spatial separation. This correlation was however recently denied
369 (Libourel et al., 2022, 2023) based on data from just two chondrules from CO3.05 chondrite
370 Yamato 81020 (since type I-CR compositions are rare there). In one of them (Ch#35; Libourel
371 et al., 2023), the type I-CR oxygen isotopic compositions are found in $\sim\text{Fo}_{99.5}$ olivine cores
372 with type I-CO overgrowths that we would rather interpret as relicts from a previous
373 generation of chondrules. They may derive from possibly originally larger grains which
374 fossilized higher-temperature, more forsteritic compositions at their (surviving) centers, as
375 observed in isolated olivine grains (Jacquet et al. 2021). Indeed, isolated olivine grains are not
376 restricted to type I-CO compositions, as those of Libourel et al. (2023) are (although virtually
377 all isolated *refractory* forsterites are type I-CO; Jacquet et al. 2021). They need not represent
378 phenocrysts of lost “megachondrules” with which Libourel et al. (2023) populate the
379 innermost regions of their impact plumes, but plausibly crystals expelled from “normal”
380 molten chondrules and which have grown on all sides by recondensation (Jacquet et al. 2021).
381 Libourel et al. (2022, 2023) do not interpret the isotopically distinct olivine cores as relicts,
382 but rather as the earliest crystallized olivine in the same chondrule-forming event (with
383 isotopically evolving ambient gas). It becomes then difficult to understand why the minor
384 element contents (and in particular the *refractory* minor elements), and thence their
385 cathodoluminescence properties (Libourel and Portail 2018) abruptly change as the isotopic
386 composition of the gas evolved and the overgrowths crystallized. Libourel et al. (2022, 2023)
387 also suggested that the literature $\text{Mg}\#-\Delta^{17}\text{O}$ correlation is an artifact of excluding putative
388 relicts. However, the said relicts are rare, and mostly ^{16}O -richer than their host, so including
389 them should not really destroy (although it does denature) the correlation. This may be
390 verified in the Marrocchi et al. (2019) compilation (their **Fig. 10** with both relict and host
391 data), bearing in mind that some Kaba (CV3.1; Bonal et al., 2006) type I olivine FeO

392 concentrations may have been increased by incipient metamorphism. Consequently, chemistry
393 and isotopic compositions are not decoupled among type I chondrules in carbonaceous
394 chondrites.

395 3– The Libourel et al. (2023) contention that type I chondrule relicts within type II
396 chondrules do not contain enstatite is erroneous (see results), so at least some type I
397 chondrules must have crystallized their whole mineral assemblage before remelting in a type
398 II chondrule-forming environment. This argues against a monotonous cooling history with
399 oxygen fugacity increasing from type I to type II territory. It must be allowed that enstatite is
400 rare in type II chondrules, when compared to forsterite, which likely marks its easier
401 remelting (because of lower melting temperature).

402 Taken together, this suggests that type I chondrules are likely nebular products formed
403 through complex processes implying recycling of early condensates, addition of dust and gas-
404 melt interactions (Schneider et al., 2020; Marrocchi et al. 2022). If correct, and considering
405 the genetic link between type I and II chondrules, this would also support a nebular origin for
406 type II chondrules. Since the bulk chemistry of type II chondrules is less devolatilized than
407 type I chondrules (e.g., Jacquet et al., 2015), the latter cannot be the sole precursors of the
408 former. We may envision type I chondrules, whole or fragmented mixed with more chondritic
409 (matrix-like) dust (see **Fig. 10**; not unlike the type I-CO to type I-CR chondrule recycling
410 scenario of Marrocchi et al., 2022) which would have been too fine-grained to survive as
411 relicts. The agglomeratic ¹⁶O-rich objects reported in CR chondrites could represent weakly
412 melted versions thereof (Schrader et al., 2018). The oxygen and silicon isotopic
413 heterogeneities observed within type II chondrules containing Mg-rich olivine relics also
414 imply open-system formation with evolving isotopic compositions being controlled by gas-
415 melt interaction processes, in agreement with their substantially enriched volatile contents
416 relative to type I chondrules.

417 In terms of astrophysical setting, it appears that the formation of type I chondrules and
418 their recycling into type II chondrules require repetitive heating mechanisms producing
419 different oxygen fugacities. Such processes must be extremely localized for producing type II
420 chondrules without recycling all type I chondrules, implying that chondrites comprise objects
421 affected by a variable number of melting episodes. These spatially-limited processes are also
422 illustrated by our data on CR chondrites where two chondrule populations characterized by
423 different sizes and oxygen isotopic compositions were recently reported (Marrocchi et al.,
424 2022). The larger, ^{16}O -poor type I-CR chondrules appear to have formed late out from
425 smaller, ^{16}O -rich type I-CO chondrules that initially populated the CR reservoir (Marrocchi et
426 al., 2022; Tenner et al., 2019). Adequate chondrule-forming scenarios in that respect are those
427 of the “nebular” brand, e.g., bow shocks induced by eccentric planetary embryos (Morris et
428 al., 2012), lightning (Johansen & Okuzumi 2017) or the short-circuit instability (McNally et
429 al. 2013).

430

431 **5- Concluding remarks**

432

433 We have determined the oxygen isotope compositions of Mg-rich relict and host
434 grains in type II chondrules in the carbonaceous chondrites Los Vientos 123 (CO3.05),
435 Catalina 008 (CO3.1), El Médano 463 and 465 (CO3), Renazzo (CR2.4) and Dar al Gani 574
436 (CR2). Our main results are:

437 1- Type II chondrules are characterized by large, mass-independent, oxygen isotope
438 variations with olivine O-isotopic composition in CO and CR chondrites ranges respectively
439 from -13.1 to $+15.2$ ‰ and -11.3 to 8.1 ‰ for $\delta^{18}\text{O}$; and from -14.2 to 5.8 ‰ and -13.1 to
440 4.4 ‰, in the case of $\delta^{17}\text{O}$. These ranges are primarily due to Mg-rich relicts generally ^{16}O -
441 richer than the hosts.

442 2- The Mg-rich relicts overlap the oxygen isotopic composition of host olivine grains
443 in type I chondrules, with the same dominant peaks shown by their respective host chondrites.
444 All analyzed relicts in CR chondrites plot around -6‰ or -2‰ for $\Delta^{17}\text{O}$ values similar to the
445 two generations of type I CR chondrules previously identified by Marrocchi et al. (2022).

446 From this, we drew the following inferences:

447 1- The oxygen isotopic composition of Mg-relicts in type II chondrules supports an
448 origin from Mg-rich type I chondrules. This points toward a genetic link between both types
449 of chondrules with type II being derived from type I chondrules *via* oxidation shocks inducing
450 the dissolution of Fe-Ni metal beads and the subsequent crystallization of FeO-rich olivine
451 overgrowths. The oxygen isotopic heterogeneity observed within type II chondrules
452 containing Mg-rich olivine relict grains also implies a formation of their precursors under
453 open-system conditions.

454 2- Combined with the presence of AOA-like ^{16}O -rich relict olivine grains and large
455 and variable nucleosynthetic anomalies previously reported in type I chondrules, our data
456 support a nebular origin of both type I and II chondrules.

457 3- As illustrated by the presence of CR type II chondrules with Mg-rich relict grains
458 having $\Delta^{17}\text{O}$ characteristics of the two chondrule generations observed in CR chondrites, our
459 data imply that the nebular process at the origin of chondrules must be extremely localized for
460 producing type II chondrules without recycling all type I chondrules.

461

462

463

464

465

466

467
468
469
470
471
472
473
474
475
476
477
478
479
480
481
482
483
484
485
486
487
488
489
490
491

Acknowledgments

Original data from this study are available on the Ordar database:
<https://doi.org/10.24396/ORDAR-93>. Nordine Bouden, Michel Fialin and Nicolas Rividi are
thanked for technical assistance. This work was funded by l'Agence Nationale de la
Recherche through grant CASSYSS ANR-18-CE31-0010-01 (PI Johan Villeneuve). This is
CRPG contribution #XXXX.

492
493
494
495
496
497
498
499
500
501

502 **Figure caption**

503
504
505
506
507
508
509
510
511
512
513
514
515
516

Fig 1: Backscattered electron images of relic-bearing type II chondrules from LoV 123 (CO3.05), Médano 465 (CO3) and (e-f) Renazzo (CR2.4). (a) LoV123_Ch02 is a relict-bearing chondrule with at least ~12 Mg-rich relict grains of various size sharply delineated from their enclosing Fe-rich olivine grains. (b) LoV123_Ch10 show abundant metal beads in the mesostasis and inside host as well as relict olivines. The central large Mg-rich relict crystal contains three rounded metal beads. (c) Ren_Ch02 is a lobate chondrule, presumably compound as suggested by the sulfide delineating the protuberance at bottom. The latter has a cluster of small Mg-rich relicts, but a bigger grain appears on the left side of the whole chondrule (possibly in another adhesion, i.e. another component chondrule; Wasson et al., 1995). (d) LoV123_Ch07 with a large (~100 μm) enstatite relict, with some olivine chadacrysts and sparse metal beads and an augitic overgrowth. (e) Ren_Ch03 is a relatively large porphyritic chondrule with the most ^{16}O -rich relict grain at $\Delta^{17}\text{O} = -7.5$ ‰. (f) The lobate chondrule

517 Ren_Ch02 display a cluster of Mg-rich olivine phenocrysts whereas each one is surrounded
518 by thin layer of Fe-rich olivine. Tro = Troilite; Kam = Kamacite; Chr = Chromite; Gyp =
519 gypsum; Fa = Fayalite; Fo = forsterite; Meso = mesostasis.

520

521 **Fig. 2:** Backscattered electron images of relic-bearing type II chondrules from LoV 123
522 (CO3.05), Médano 465 (CO3). (a-b) LoV123_Ch18 displays several Mg-rich olivine crystals
523 sparsely distributed over its area and in the center a metal-bearing IBA chondrule relict
524 intruded by an olivine-microlite rich mesostasis of the host. (c) LoV123_Ch11 is a large Fe-
525 rich chondrule (~500 μm) containing a central region with large (>200 μm) partly embayed
526 euhedral olivine phenocrysts, a nonporphyritic right bottom region and two relict-bearing
527 olivine clusters at the top, one with coarse forsterites (near the middle) and another with a
528 olivine-chadacryst-bearing enstatite crystal. Possibly the latter was an independent partly
529 melted droplet which collided with a coarser-grained one. (d) LoV123_Ch15, fine grained
530 (“agglomeratic”; e.g. Schrader et al. 2018) type II chondrule with a sulfide-rich outer region
531 and a large, elongate type IAB porphyritic chondrule-textured relict (~120 μm), with partly
532 oxidized metal beads. (e) EM465_Ch04 display a type I POP-textured relict, with (olivine
533 chadacryst-laden) enstatite dominating toward its margin (the top protuberance may be an
534 adhesion merged with the main type I chondrule during its original formation episode) and
535 olivine grains displaying thin Fe-rich margins. Other magnesian relict grains occur sparsely
536 throughout the host. Some porosities are filled by (light gray) gypsum. (f) EM465_Ch05
537 shows a cluster of Mg-rich relicts on the right, possibly a late adhesion on the main chondrule,
538 and other sparsely distributed relicts, possibly making a second cluster near the lower left .
539 The porosity is filled by anhedral massive gypsum. Spot analysis in SIMS is indicated as
540 orange and blue circles for relict and host olivines. Tro = Troilite; Kam = Kamacite; Chr =
541 Chromite; Gyp = gypsum; Fa = Fayalite; Fo = forsterite; Meso = mesostasis.

542

543 **Fig 3:** (a) Triple oxygen isotope plot of the olivine crystals in the 13 analyzed Fe-rich
544 chondrules. Relict grains show mass-independent variations plotting along the Primary
545 Chondrule Mineral (PCM) line. (b-e) $\Delta^{17}\text{O}$ values vs. (b) Al_2O_3 (c) CaO , (d) Cr_2O_3 , (e) MnO
546 and (f) Olivine Fa content ($=\text{Fe}/[\text{Mg} + \text{Fe}] \times 100$ mol%) in log scale. The estimated
547 composition of type I and type II chondrules and the Terrestrial Fractionation line (TFL;
548 Clayton et al., 1991) are shown for reference.

549

550 **Fig 4:** Oxygen three-isotope diagrams for type II chondrules from (a–h) CO and (i–m) CR
551 chondrites. Reference lines are Terrestrial Fractionation (TF; Clayton et al., 1991), and the
552 Primitive Chondrule Minerals (PCM; Ushikubo et al., 2012). The error bars are smaller than
553 marker size.

554

555 **Fig. 5:** Curves show probability density function of $\Delta^{17}\text{O}$ of type I host olivines and type II
556 Mg-relict grains in both CO (a) and CR chondrites (b). Data from this study, Schrader et al.
557 (2013); Tenner et al. (2013, 2015); Fukuda et al., (2022); Kunihiro et al. (2004) and Libourel
558 et al. (2022, 2023).

559

560 **Fig 6.** The Mg# - $\Delta^{17}\text{O}$ value of relict and host olivines in type I and type II chondrules from
561 CO (a) and CR (b) chondrites. Fa content ($=100 \times \text{Fe}/[\text{Mg} + \text{Fe}]$) is plotted in log scale
562 revealing a transition and overlapping between olivine grains in type I chondrules and relict
563 grains in type II chondrules for carbonaceous chondrites. The probability density function of
564 relict and host grains in type I and II chondrules are show to the right of each chondrite group.
565 Errors are 2σ . Data of type I chondrules in carbonaceous chondrites are from Schrader et al.
566 (2013); Kunihiro et al. (2004); Tenner et al. (2013); Hertwig et al. (2018); Chaumard et al.

567 (2018); Marrocchi et al. (2018, 2019, 2022); and Libourel et al. (2022, 2023). The TFL is
568 shown as blue line for reference.

569

570 **Fig. 7:** The $\Delta^{17}\text{O}$ value plotted against Al_2O_3 (a), CaO (b), Cr_2O_3 (c), and MnO (d) for relict
571 and host olivines in type I and II chondrules from CO, CV, CM and C2-an carbonaceous
572 chondrites. The TFL is shown as blue line for reference. Errors are 2σ . Data of type I and II
573 chondrules of CO, CV, CM and C2-an carbonaceous chondrites from Kunihiro et al. (2004);
574 Tenner et al. (2013); Libourel et al. (2022,2023); Hertwig et al. (2018); Chaumard et al.
575 (2018); Marrocchi et al. (2018, 2019). Data of type II chondrules are show in blue and
576 skyblue for this study and literature data, respectively.

577 **Fig. 8:** The $\Delta^{17}\text{O}$ value plotted against Al_2O_3 (a), CaO (b), Cr_2O_3 (c), and MnO (d) for relict
578 and host olivines in type I and II chondrules from CR carbonaceous chondrites. The TFL is
579 shown as blue line for reference. Errors are 2σ . Data of type I and II chondrules from
580 Schrader et al. (2013) and Marrocchi et al. (2022). Data of type II chondrules are show in
581 green and light green for this study and literature data, respectively.

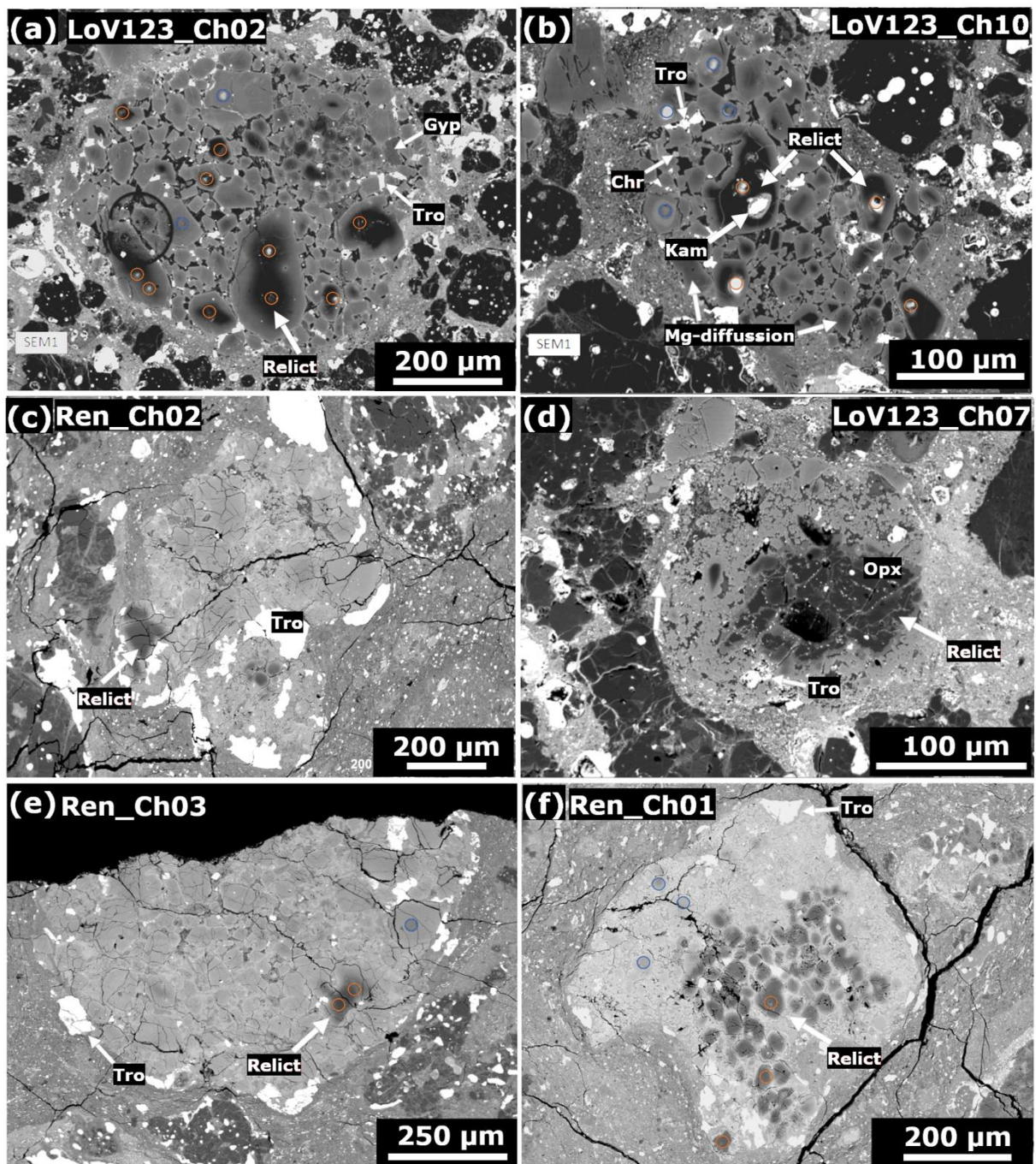
582

583 **Fig. 9:** Schematic representation of formation of type I and II chondrules in CO chondrites.
584 Previously condensed ^{16}O -rich AOAs mixed with NC-like dust before experienced
585 subsequent melting and gas-melt interactions. This lead to the formation of olivine-rich type I
586 chondrules characterized by ^{50}Ti - ^{54}Cr anomalies and the presence of ^{16}O -rich olivine grains.
587 Depending on the duration of gas-melt interaction, PO, POP or PP type I chondrules are
588 formed. Later heating event under oxidizing conditions induced the formation of type II
589 chondrules. Depending on duration of the oxidation shock, Mg-rich olivine grains can be
590 either conserved or fully dissolved.

591

592 **Fig. 10:** Schematic representation of formation of type I and II chondrules in CR chondrites.
593 Similarly to CO chondrules, small type I CR chondrules result from the melting of a mix of
594 ¹⁶O-rich AOAs and NC-like dust followed by gas-melt interactions. A second generation of
595 large type I chondrules were also formed through the recycling of CI-like dust, inducing the
596 presence of two chondrule generations in CR chondrites. Both type of type I CR chondrules
597 were then recycled into type II chondrules with Mg-rich relict grains having $\Delta^{17}\text{O}$
598 characteristics of the two generations of type I chondrule. This implies that the origin of
599 chondrules must be extremely localized for producing type II chondrules without recycling all
600 type I chondrules.

601



602

603

604

605

606

607

608

Fig. 1

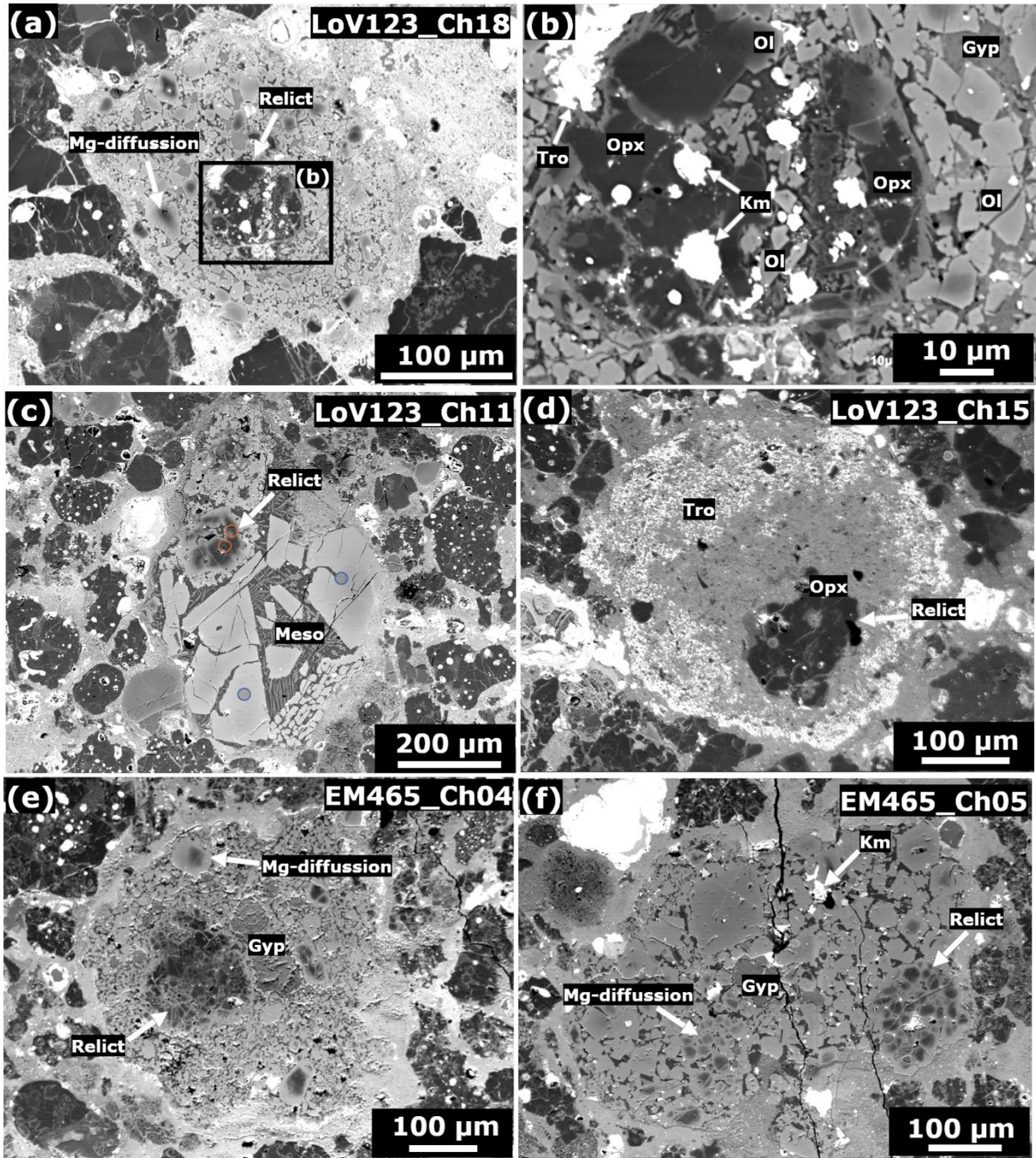
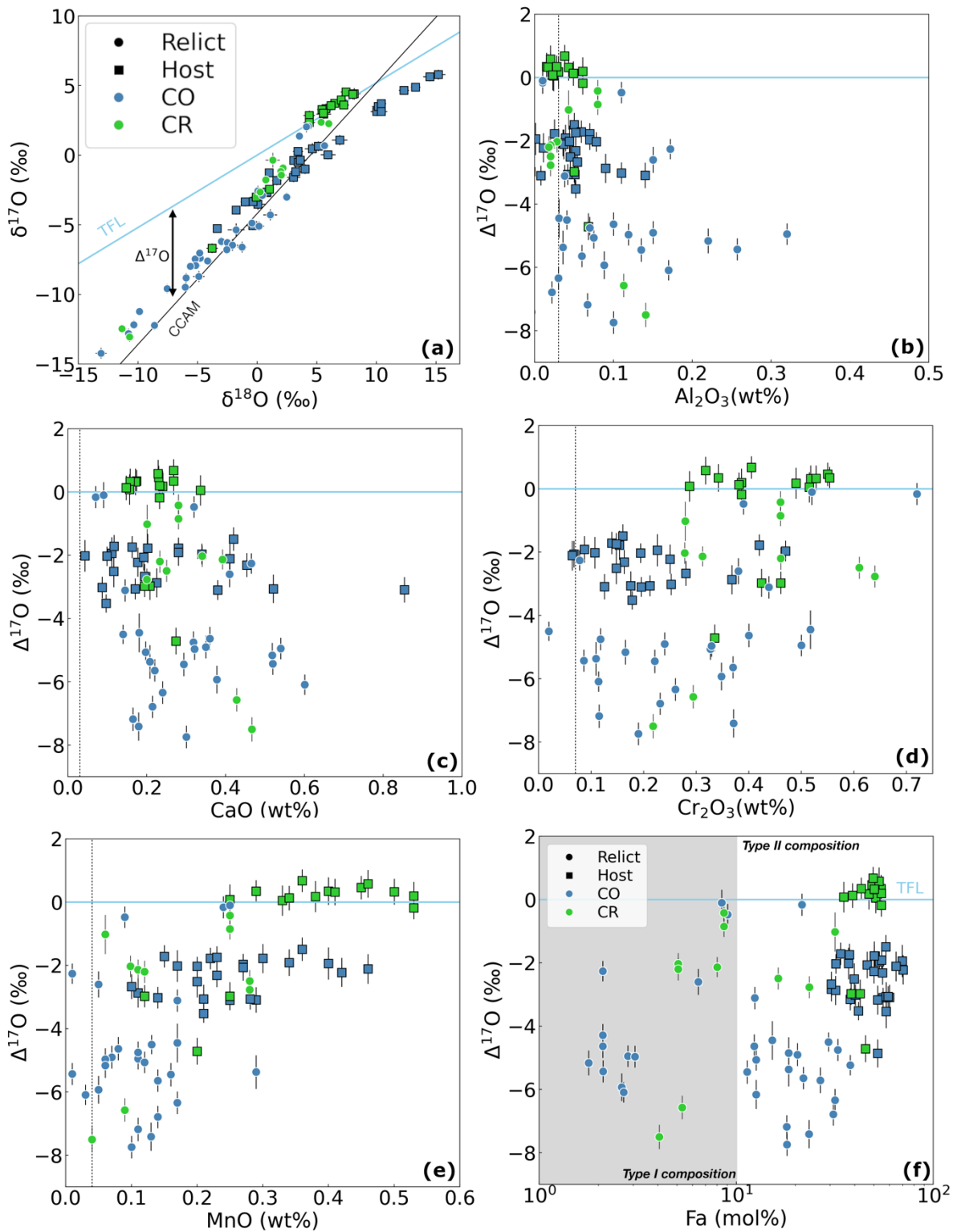


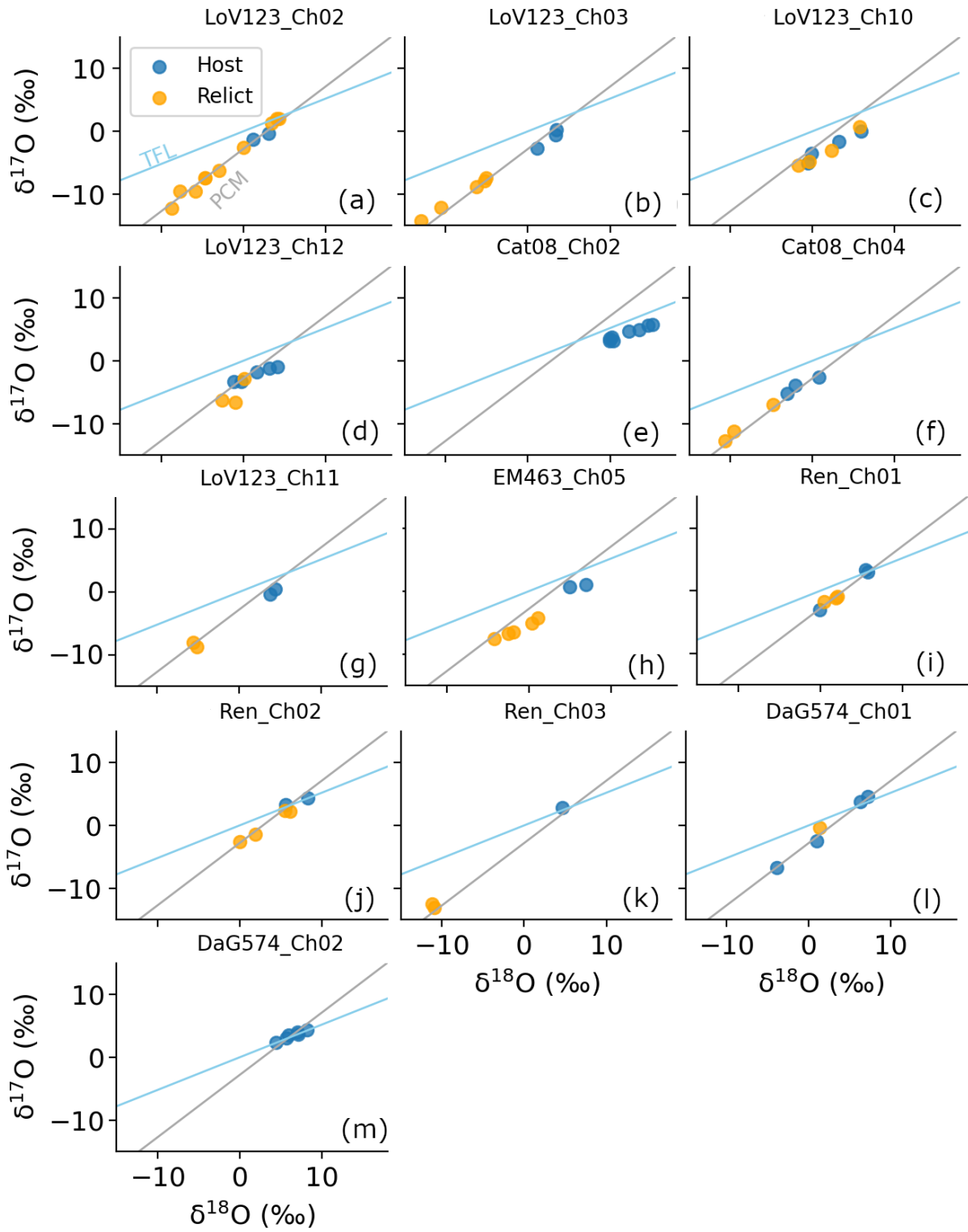
Fig. 2

609
610
611
612
613
614



615
 616
 617
 618

Fig. 3



619
 620
 621
 622
 623
 624
 625
 626

Fig. 4

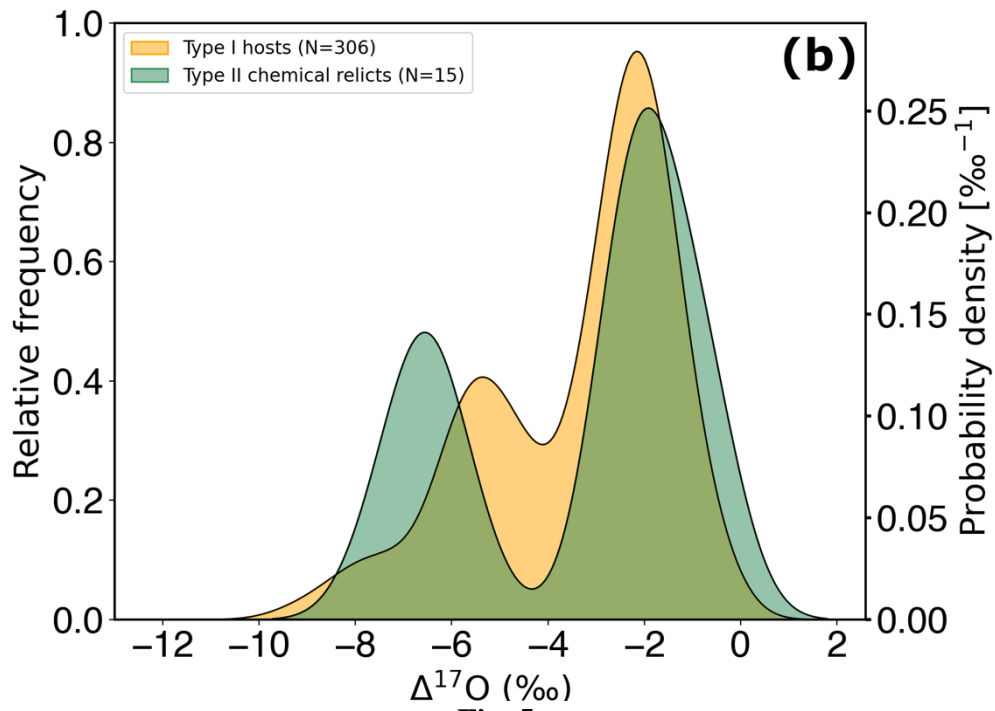
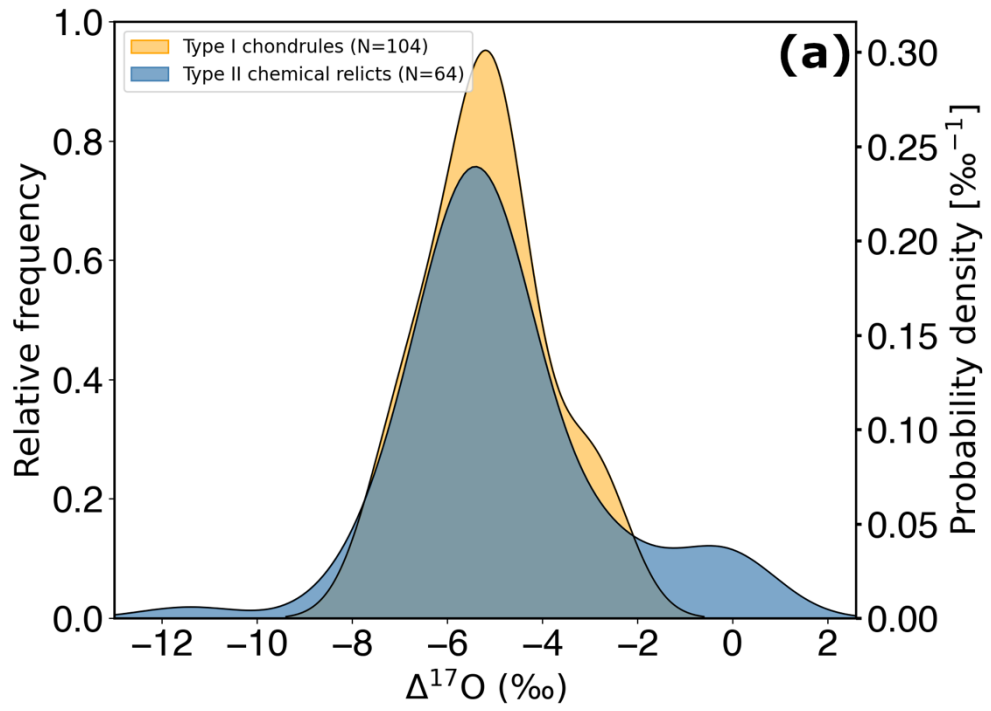


Fig. 5

627
628
629
630
631

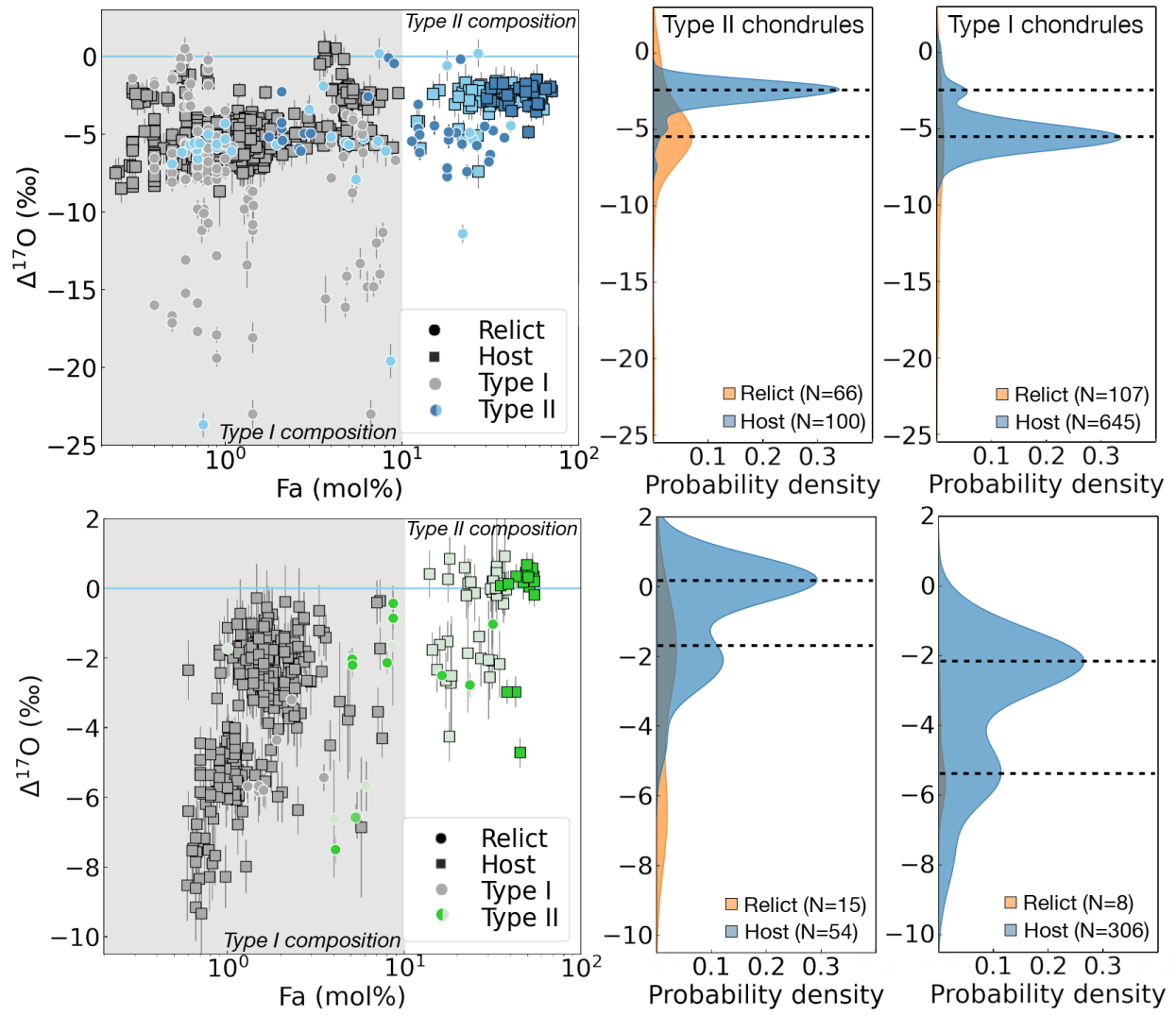


Fig. 6

632

633

634

635

636

637

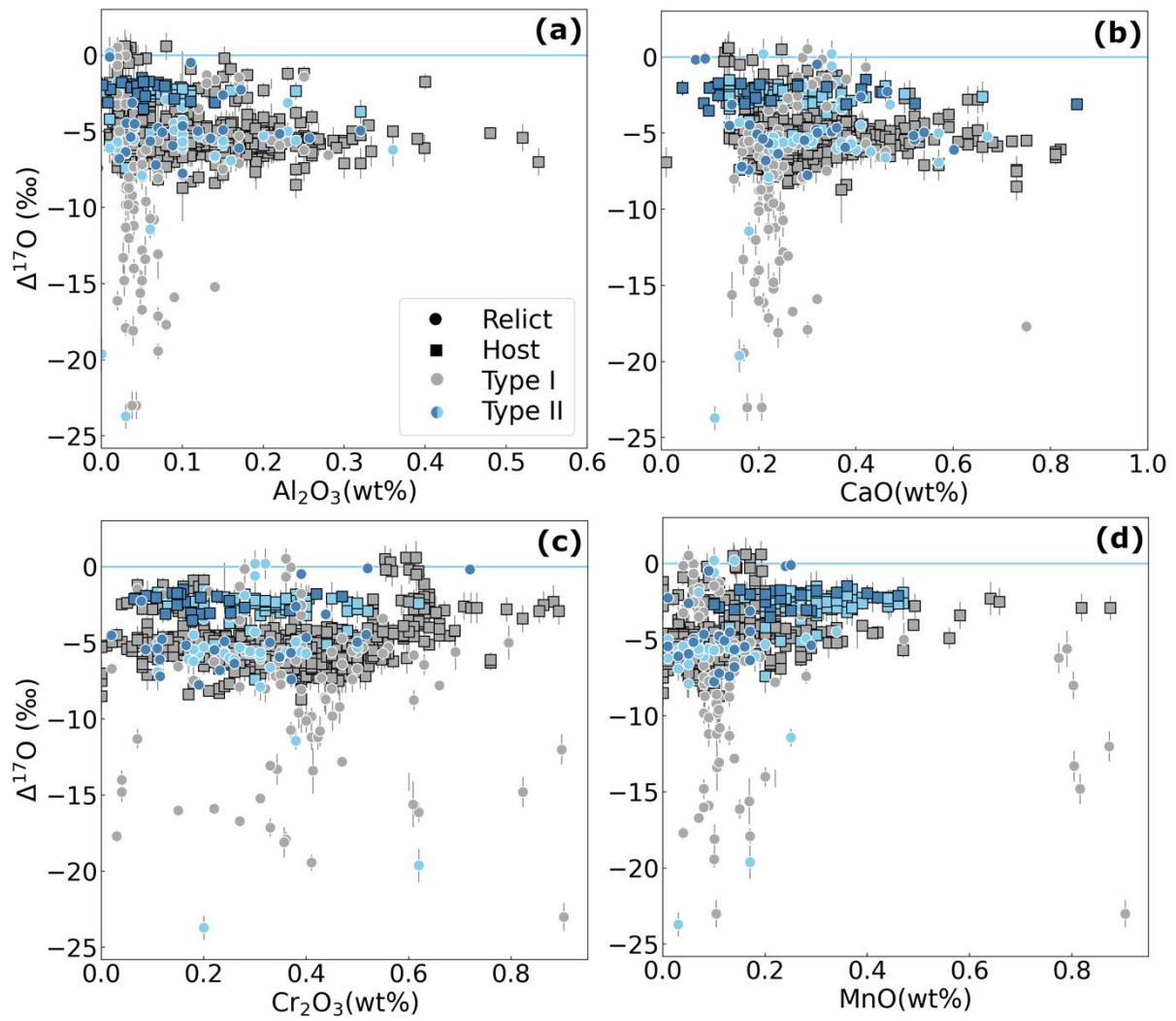


Fig. 7

638

639

640

641

642

643

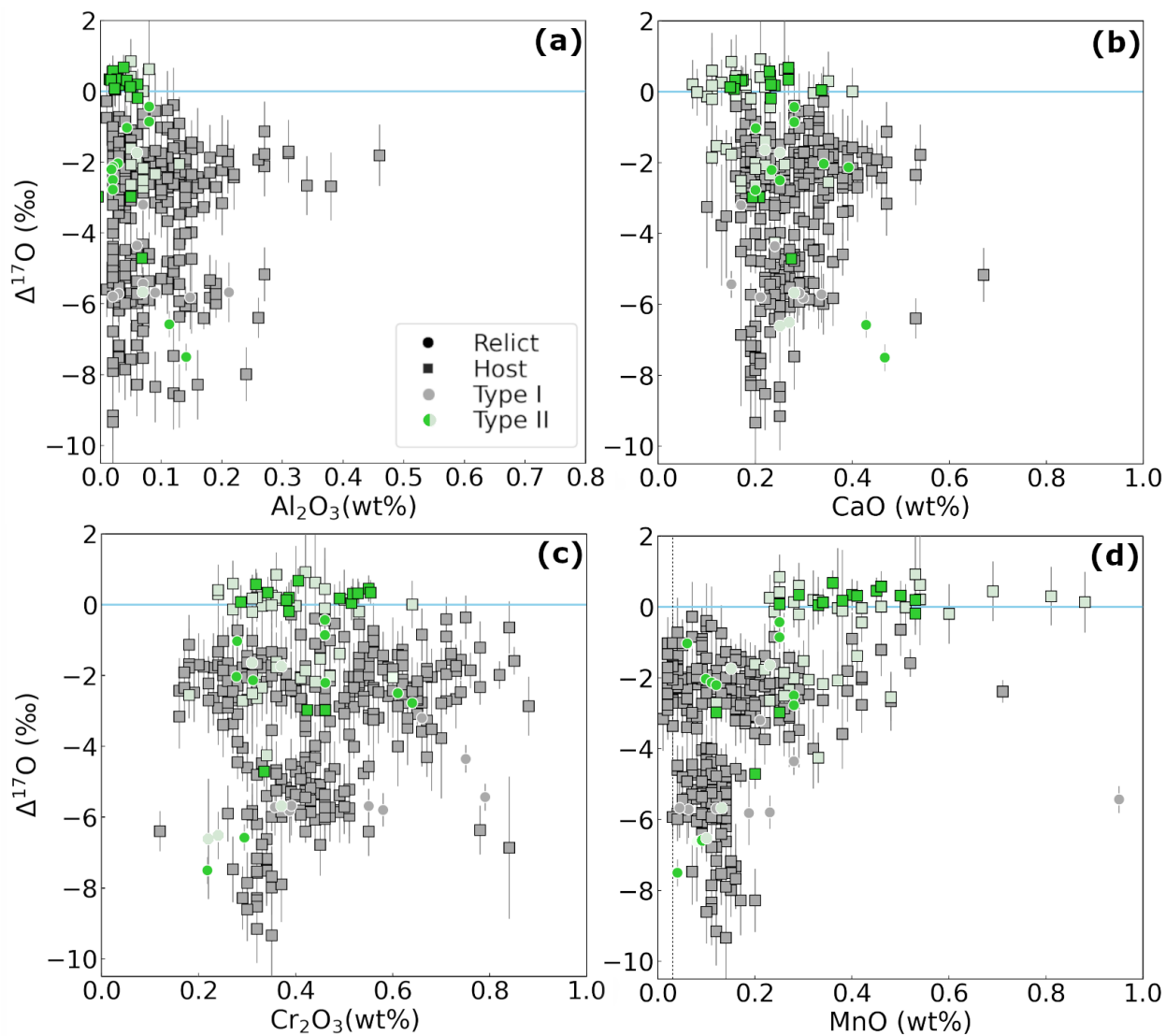


Fig. 8

644
 645
 646
 647
 648
 649
 650
 651
 652
 653
 654
 655
 656

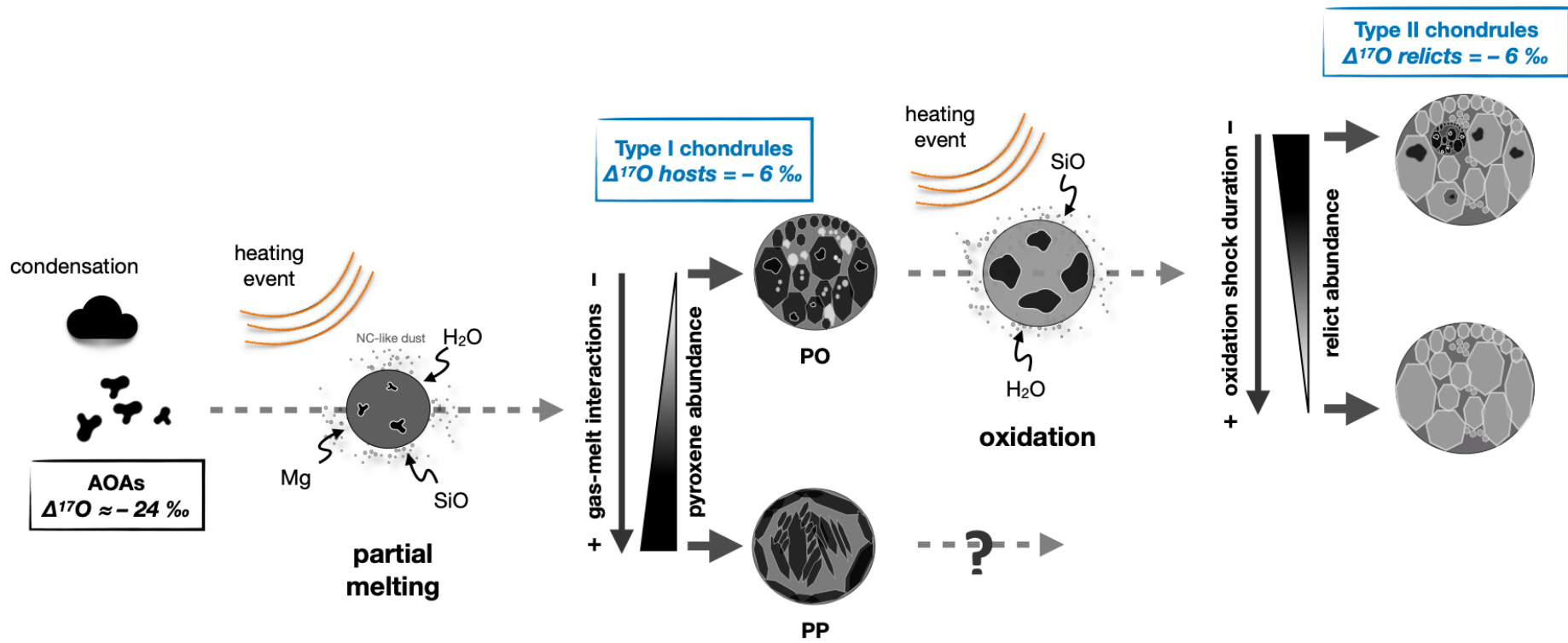


Fig. 9

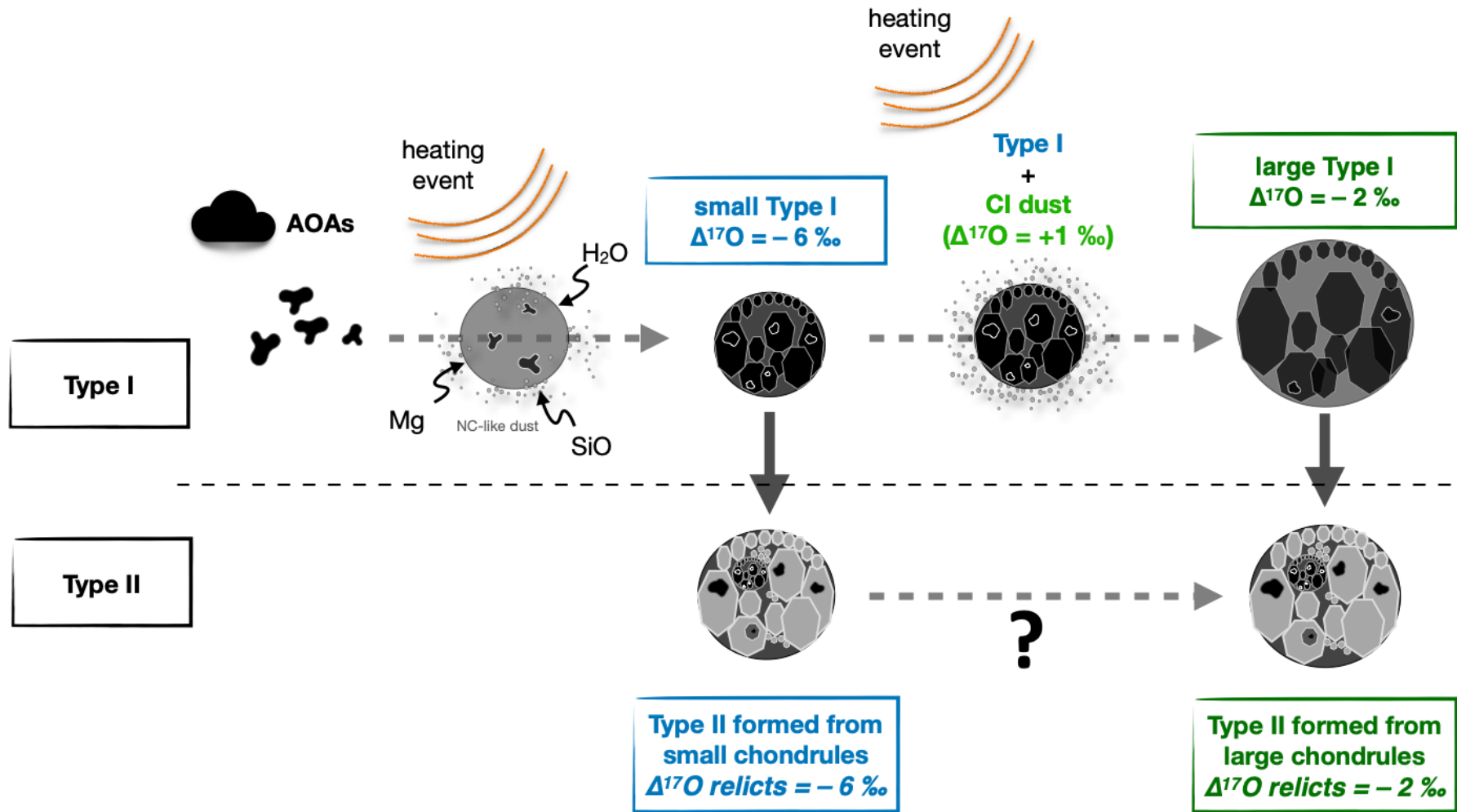


Fig. 10

Table 1. Mean major and minor composition of 688 spot analysis in host and relict olivine grains among the 13 studied FeO-rich chondrules.

Class	Meteorite	Chondrule	Grain type	N	Mg# (mol%)	MgO	Al ₂ O ₃	SiO ₂	CaO	TiO ₂	Cr ₂ O ₃	MnO	FeO	
CO	<i>LoV123</i>	<i>Ch_02</i>	Host	82	51.66	35.52	0.08	37.64	0.35	0.01	0.34	0.23	26.00	
			Relict	53	82.78	50.29	0.07	41.34	0.25	0.04	0.37	0.16	8.27	
		<i>Ch_12</i>	Host	44	49.40	33.93	0.14	37.03	0.47	0.01	0.30	0.24	27.40	
			Relict	20	87.83	52.17	0.09	41.59	0.41	0.03	0.33	0.09	5.92	
		<i>Ch_03</i>	Host	72	45.09	31.63	0.15	36.56	0.50	0.02	0.26	0.27	30.04	
			Relict	23	72.86	46.04	0.03	39.72	0.34	0.02	0.27	0.14	13.40	
		<i>Ch_10</i>	Host	22	42.87	30.00	0.28	36.00	0.45	0.02	0.37	0.23	31.22	
			Relict	14	90.20	52.33	0.11	41.74	0.33	0.04	0.49	0.04	4.49	
		<i>Ch_11</i>	Host	49	29.54	22.05	0.01	34.34	0.18	b.d.	0.27	0.42	40.98	
	Relict		7	84.77	50.41	0.07	40.69	0.23	0.04	0.29	0.14	7.32		
	<i>Cat 008</i>	<i>Ch_02</i>	Host	108	51.32	34.98	0.07	37.49	0.22	0.01	0.18	0.28	26.40	
			Host	50	48.16	33.62	0.06	37.21	0.17	0.01	0.14	0.23	28.57	
			Relict	20	84.62	51.20	0.10	41.63	0.37	0.05	0.13	0.08	7.47	
	<i>EM463</i>	<i>Ch_05</i>	Host	41	52.77	35.85	0.13	37.95	0.17	0.01	0.16	0.25	25.33	
			Relict	52	88.64	52.40	0.17	41.67	0.39	0.05	0.14	0.07	5.36	
	CR	<i>Renazzo</i>	<i>Ch_01</i>	Host	4	52.17	35.76	0.01	37.50	0.26	0.02	0.41	0.31	25.52
				Relict	3	93.94	54.93	0.02	41.96	0.32	0.03	0.35	0.11	2.75
			<i>Ch_02</i>	Host	3	53.29	36.07	0.02	37.44	0.19	0.04	0.46	0.37	24.54

		Relict	4	81.57	49.41	0.03	41.02	0.23	0.01	0.55	0.27	8.77
	<i>Ch_03</i>	Host	3	46.16	32.38	0.02	36.86	0.26	0.01	0.38	0.43	29.30
		Relict	3	83.45	49.82	0.08	41.41	0.36	0.06	0.30	0.13	8.28
	<i>DaG 574</i>											
	<i>Ch_01</i>	Host	4	55.97	37.99	0.05	38.25	0.23	0.01	0.44	0.24	23.24
		Relict	2	69.09	44.43	0.08	39.39	0.23	0.07	0.39	0.11	15.42
	<i>Ch_02</i>	Host	5	54.17	37.16	0.04	38.11	0.17	b.d.	0.42	0.40	24.58

b.d.:below detection limit

Table 2. Compilation of mean Mg#s and oxygen isotope ratios of 88 spot analysis in the 13 FeO-rich chondrules from the carbonaceous chondrite LoV 123 (CO3.05), Cat 008 (CO3.1), EM 463 (CO3.2), Renazzo (CR2.4), and DaG 574 (CR2). $\delta^{17}\text{O}$ and $\delta^{18}\text{O}$ are relative to VSMOW (Vienna Standard Mean Ocean Water).

Class	Chondrite	Chondrule	Grain type	N analysis	$\delta^{18}\text{O}$ (‰)	2σ	$\delta^{17}\text{O}$ (‰)	2σ	$\Delta^{17}\text{O}$ (‰)	2σ	Mg# (mol%)		
CO	LoV123	Ch02	Relict	10	-2.27	0.31	-4.94	0.33	-3.75	0.37	84.74		
			Host	2	2.03	0.33	-0.81	0.29	-1.87	0.33	48.29		
		Ch03	Relict	5	-7.96	0.37	-10.12	0.32	-5.98	0.38	69.62		
			Host	3	2.56	0.39	-0.97	0.29	-2.30	0.35	43.91		
		Ch10	Relict	4	1.48	0.43	-3.14	0.35	-3.91	0.42	94.61		
			Host	4	2.17	0.60	-2.53	0.35	-3.66	0.47	45.09		
		Ch11	Relict	2	-5.26	0.40	-8.34	0.34	-5.61	0.40	87.39		
			Host	2	4.12	0.58	0.06	0.38	-2.08	0.49	30.16		
		Ch12	Relict	3	-1.13	0.36	-5.25	0.33	-4.67	0.38	93.97		
			Host	5	1.50	0.41	-2.14	0.34	-2.92	0.40	61.91		
		Cat008	Ch02	Host	8	12.04	0.49	4.31	0.30	-1.95	0.40	53.85	
				Ch04	Relict	3	-8.50	0.31	-10.34	0.29	-5.92	0.33	83.31
					Host	3	-1.44	0.32	-3.95	0.27	-3.20	0.32	53.06
		EM463	Ch05	Relict	6	-2.04	0.45	-6.37	0.34	-5.31	0.41	89.51	
				Host	2	6.02	0.67	0.87	0.36	-2.26	0.50	61.63	
		CR	Renazzo	Ch01	Relict	3	1.61	0.35	-1.28	0.28	-2.12	0.34	93.94
					Host	3	3.75	0.55	1.10	0.35	-0.85	0.45	50.71

<i>DaG574</i>	<i>Ch02</i>	Relict	4	3.40	0.36	0.14	0.29	-1.63	0.35	85.73
		Host	2	6.78	0.47	3.85	0.41	0.32	0.43	52.03
	<i>Ch03</i>	Relict	2	-11.02	0.36	-12.76	0.32	-7.03	0.37	95.31
		Host	1	4.36	0.49	2.85	0.36	0.58	0.44	46.87
	<i>Ch01</i>	Relict	1	1.30	0.61	-0.35	0.53	-1.02	0.62	68.32
		Host	4	2.79	0.43	-0.21	0.30	-1.66	0.37	55.97
	<i>Ch02</i>	Host	6	6.41	0.47	3.48	0.34	0.15	0.42	52.74

References

- Berlin, J., Jones, R. H., & Brearley, A. J. (2011). Fe-Mn systematics of type IIA chondrules in unequilibrated CO, CR, and ordinary chondrites. *Meteoritics and Planetary Science*, 46(4), 513–533. <https://doi.org/10.1111/j.1945-5100.2011.01171.x>
- Bollard, J., Connelly, J. N., Whitehouse, M. J., Pringle, E. A., Bonal, L., Jørgensen, J. K., Nordlund, Å., Moynier, F., & Bizzarro, M. (2017). Early formation of planetary building blocks inferred from Pb isotopic ages of chondrules. *Science Advances*, 3(8), 1–23. <https://doi.org/10.1126/sciadv.1700407>
- Bonal, L., Quirico, E., Bourot-Denise, M., & Montagnac, G. (2006). Determination of the petrologic type of CV3 chondrites by Raman spectroscopy of included organic matter. *Geochimica et Cosmochimica Acta*, 70(7), 1849–1863. <https://doi.org/10.1016/j.gca.2005.12.004>
- Bouden, N., Villeneuve, J., Marrocchi, Y., Deloule, E., Füri, E., Gurenko, A., Piani, L., Thomassot, E., Peres, P., & Fernandes, F. (2021). Triple Oxygen Isotope Measurements by Multi-Collector Secondary Ion Mass Spectrometry. *Frontiers in Earth Science*, 8, 1–9. <https://doi.org/10.3389/feart.2020.601169>
- Burkhardt, C., Jansen, C., Marrocchi, Y., Schneider, J. M., Wölfer, E., & Kleine, T. (2023, July). *Isotopic evidence for a common origin of CAIs and AOs*. In Goldschmidt Conference, Lyon, France.
- Chaumard, N., Defouilloy, C., Hertwig, A. T., & Kita, N. T. (2021). Oxygen isotope systematics of chondrules in the Paris CM2 chondrite: Indication for a single large formation region across snow line. *Geochimica et Cosmochimica Acta*, 299, 199–218. <https://doi.org/10.1016/j.gca.2021.02.012>
- Chaumard, N., Defouilloy, C., & Kita, N. T. (2018). Oxygen isotope systematics of chondrules in the Murchison CM2 chondrite and implications for the CO-CM relationship. *Geochimica et Cosmochimica Acta*, 228, 220–242. <https://doi.org/10.1016/j.gca.2018.02.040>
- Clayton, R. N., Mayeda, T. K., Goswami, J. N., & Olsen, E. J. (1991). Oxygen isotope studies of ordinary chondrites. *Geochimica et Cosmochimica Acta*, 55(8), 2317–2337. [https://doi.org/10.1016/0016-7037\(91\)90107-G](https://doi.org/10.1016/0016-7037(91)90107-G)
- Connolly, H. C., Hewins, R. H., Ash, R. D., Zanda, B., Lofgren, G. E., & Bourot-Denise, M. (1994). Carbon and the formation of reduced chondrules. *Nature*, 371(6493), 136–139. <https://doi.org/10.1038/371136a0>
- Connolly H. C. and Jones R. H. (2016). Chondrules: the canonical and noncanonical views. *J. Geophys. Res. Planets* 121, 1885–1899. <https://doi.org/10.1002/2016JE005113>
- Ebel, D. S., Alexander, C. M. O., & Libourel, G. (2018). Vapor – Melt Exchange Constraints on Chondrite Formation Conditions. In *Chondrules: Records of Protoplanetary Disk Processes*. Cambridge University Press, pp. 151–174.
- Fukuda, K., Tenner, T.J., Kimura, M., Tomioka, N., Siron, G., Ushikubo, T., Chaumard, N., Hertwig, A.T., Kita, N.T., 2022. A temporal shift of chondrule generation from the inner to outer Solar System inferred from oxygen isotopes and Al-Mg chronology of chondrules from primitive CM and CO chondrites. *Geochim. Cosmochim. Acta* 322, 194–226.
- Gerber, S., Burkhardt, C., Budde, G., Metzler, K., & Kleine, T. (2017). Mixing and transport of dust in the early solar nebula as inferred from titanium isotope variations among chondrules. *The Astrophysical Journal Letters*, 841(1), 7. <https://doi.org/10.3847/2041-8213/aa72a2>

- Han, J., & Brearley, A. J. (2015). Microstructural evidence for complex formation histories of amoeboid olivine aggregates from the ALHA77307 CO3.0 chondrite. *Meteoritics and Planetary Science*, 50(5), 904–925. <https://doi.org/10.1111/maps.12439>
- Hertwig, A. T., Defouilloy, C., & Kita, N. T. (2018). Formation of chondrules in a moderately high dust enriched disk: Evidence from oxygen isotopes of chondrules from the Kaba CV3 chondrite. *Geochimica et Cosmochimica Acta*, 224, 116–131. <https://doi.org/10.1016/j.gca.2017.12.013>
- Hewins R. H., Connolly H. C., Logfren G. E. J. and Libourel G. (2005) Experimental constraints on chondrules formation. In *Chondrites and the Protoplanetary Disk*. ASP Conference Series, vol. 341 (eds. Alexander N. Krot, Edward R. D. Scott and B Reipurth). Astronomical Society of the Pacific, San Francisco, p. 286.
- Hewins, R. H., & Zanda, B. (2012). Chondrules: Precursors and interactions with the nebular gas. *Meteoritics and Planetary Science*, 47(7), 1120–1138. <https://doi.org/10.1111/j.1945-5100.2012.01376.x>
- Jacquet, E. (2021). Collisions and compositional variability in chondrule-forming events. *Geochimica et Cosmochimica Acta*, 296, 18–37. <https://doi.org/10.1016/j.gca.2020.12.025>
- Jacquet, E., Alard, O., & Gounelle, M. (2015). Trace element geochemistry of ordinary chondrite chondrules: The type I/type II chondrule dichotomy. *Geochimica et Cosmochimica Acta*, 155, 47–67. <https://doi.org/10.1016/j.gca.2015.02.005>
- Jacquet, E., & Marrocchi, Y. (2017). Chondrule heritage and thermal histories from trace element and oxygen isotope analyses of chondrules and amoeboid olivine aggregates. *Meteoritics and Planetary Science*, 52(12), 2672–2694. <https://doi.org/10.1111/maps.12985>
- Jacquet, E., Piralla, M., Kersaho, P., & Marrocchi, Y. (2021). Origin of isolated olivine grains in carbonaceous chondrites. *Meteoritics & Planetary Science*, 56, 13–33. <https://doi.org/10.1111/maps.13583>
- Johansen, A., & Okuzumi, S. (2017, March). *Harvesting the Decay Energy of 26-Al to Drive Lightning Discharge and Chondrule Formation*. Lunar and Planetary Conference, The Woodlands, Texas, USA. Contrib. No. 1963
- Johnson, B. C., Minton, D. A., Melosh, H. J., & Zuber, M. T. (2015). Impact jetting as the origin of chondrules. *Nature*, 517(7534), 339–341. <https://doi.org/10.1038/nature14105>
- Jones, R. H. (1996). Relict Grains in Chondrules: Evidence for Chondrule Recycling. In *Chondrules and the Protoplanetary Disk*, edited by R. H. Hewins, R. H. Jones, & Scott. Cambridge, UK: Cambridge University Press, Vol. 1, pp. 163–172.
- Jones, R. H. (2012). Petrographic constraints on the diversity of chondrule reservoirs in the protoplanetary disk. *Meteoritics and Planetary Science*, 47(7), 1176–1190. <https://doi.org/10.1111/j.1945-5100.2011.01327.x>
- Jones, R. H., Leshin, L. A., & Guan, Y. (2002). Heterogeneity and ¹⁶O-enrichments in oxygen isotope ratios of olivine from chondrules in the mokoia CV3 chondrite. *Lunar and Planetary Conference*, 1571.
- Jones, R. H., Villeneuve, J., & Libourel, G. (2018). Thermal Histories of Chondrules: Petrologic Observations and Experimental Constraints. In *Chondrules: Records of Protoplanetary Disk Processes*. Cambridge University Press, pp. 57–90.
- Kita, N.T., Fukuda, K., Tenner T.J, Zhang, M., Kimura M. (2022). *Correlation between mass independent oxygen isotope fractionation and Mg# among type I chondrules in pristine CO chondrite DOM 08006*. In Goldschmidt Conference, Hawai, USA.

- Krot, A. N. (2019). Refractory inclusions in carbonaceous chondrites: Records of early solar system processes. *Meteoritics and Planetary Science*, 54(8), 1647–1691. <https://doi.org/10.1111/maps.13350>
- Krot, A. N., Petaev, M. I., Russell, S. S., Itoh, S., Fagan, T. J., Yurimoto, H., Chizmadia, L., Weisberg, M. K., Komatsu, M., Ulyanov, A. A., & Keil, K. (2004). Amoeboid olivine aggregates and related objects in carbonaceous chondrites: Records of nebular and asteroid processes. *Chemie Der Erde*, 64(3), 185–239. <https://doi.org/10.1016/j.chemer.2004.05.001>
- Kruijer, T. S., Burkhardt, C., Budde, G., & Kleine, T. (2017). Age of Jupiter inferred from the distinct genetics and formation times of meteorites. *Proceedings of the National Academy of Sciences of the United States of America*, 114(26), 6712–6716. <https://doi.org/10.1073/pnas.1704461114>
- Kunihiro, T., Rubin, A. E., McKeegan, K. D., & Wasson, J. T. (2004). Oxygen-isotopic compositions of relict and host grains in chondrules in the Yamato 81020 CO3.0 chondrite. *Geochimica et Cosmochimica Acta*, 68(17), 3599–3606. <https://doi.org/10.1016/j.gca.2004.02.011>
- Kunihiro, T., Rubin, A. E., & Wasson, J. T. (2005). Oxygen-isotopic compositions of low-FeO relicts in high-FeO host chondrules in Acfer 094, a type 3.0 carbonaceous chondrite closely related to CM. *Geochimica et Cosmochimica Acta*, 69(15), 3831–3840. <https://doi.org/10.1016/j.gca.2005.01.031>
- Libourel, G., & Krot, A. N. (2007). Evidence for the presence of planetesimal material among the precursors of magnesian chondrules of nebular origin. *Earth and Planetary Science Letters*, 254(1–2), 1–8. <https://doi.org/10.1016/j.epsl.2006.11.013>
- Libourel, G., Nagashima, K., Portail, M., & Krot, A. N. (2022). Oxygen isotope variations in Mg-rich olivines from type I chondrules in carbonaceous chondrites. *Geochimica et Cosmochimica Acta*, 319, 73–93. <https://doi.org/10.1016/j.gca.2021.12.026>
- Libourel, G., Nagashima, K., Portail, M., & Krot, A. N. (2023). On the significance of oxygen-isotope variations in chondrules from carbonaceous chondrites. *Geochimica et Cosmochimica Acta*, 346, 102–120. <https://doi.org/10.1016/j.gca.2023.01.026>
- Libourel, G., & Portail, M. (2018). Chondrules as direct thermochemical sensors of solar protoplanetary disk gas. *Science Advances*, 4(7). <https://doi.org/10.1126/sciadv.aar3321>
- Marrocchi, Y., Euverte, R., Villeneuve, J., Batanova, V., Welsch, B., Ferrière, L., & Jacquet, E. (2019b). Formation of CV chondrules by recycling of amoeboid olivine aggregate-like precursors. *Geochimica et Cosmochimica Acta*, 247, 121–141. <https://doi.org/10.1016/j.gca.2018.12.038>
- Marrocchi, Y., Piralla, M., Regnault, M., Batanova, V., Villeneuve, J., & Jacquet, E. (2022). Isotopic evidence for two chondrule generations in CR chondrites and their relationships to other carbonaceous chondrites. *Earth and Planetary Science Letters*, 593, 117683. <https://doi.org/10.1016/j.epsl.2022.117683>
- Marrocchi, Y., Villeneuve, J., Batanova, V., Piani, L., & Jacquet, E. (2018). Oxygen isotopic diversity of chondrule precursors and the nebular origin of chondrules. *Earth and Planetary Science Letters*, 496, 132–141. <https://doi.org/10.1016/j.epsl.2018.05.042>
- Marrocchi, Y., Villeneuve, J., Jacquet, E., Piralla, M., & Chaussidon, M. (2019a). Rapid condensation of the first Solar System solids. *Proceedings of the National Academy of Sciences of the United States of America*, 116(47), 23461–23466. <https://doi.org/10.1073/pnas.1912479116>
- McNally, C. P., Hubbard, A., Mac Low, M. M., Ebel, D. S., & D'Alessio, P. (2013, July). *Thermal Processing of Solids through the Short Circuit Instability*. In Protostars and Planets VI, Heidelberg, Germany.

- Morris, M. A., Boley, A. C., Desch, S. J., & Athanassiadou, T. (2012). Chondrule formation in bow shocks around eccentric planetary embryos. *Astrophysical Journal*, 752(1). <https://doi.org/10.1088/0004-637X/752/1/27>
- Piralla, M., Villeneuve, J., Batanova, V., Jacquet, E., & Marrocchi, Y. (2021). Conditions of chondrule formation in ordinary chondrites. *Geochimica et Cosmochimica Acta*, 313, 295–312. <https://doi.org/10.1016/j.gca.2021.08.007>
- Piralla, M., Villeneuve, J., Schnuriger, N., Bekaert, D. V., & Marrocchi, Y. (2023). A unified chronology of dust formation in the early solar system. *Icarus*, 394, 115427. <https://doi.org/10.1016/j.icarus.2023.115427>
- Pouchou, L. J. and Pichoir, F., 1984. New model quantitative x-ray microanalysis, 1. Application to the analysis of homogeneous samples. *Rech. Aerosp.* **3**, 13-38.
- Ruzicka, A., Floss, C., & Hutson, M. (2008). Relict olivine grains, chondrule recycling, and implications for the chemical, thermal, and mechanical processing of nebular materials. *Geochimica et Cosmochimica Acta*, 72(22), 5530–5557. <https://doi.org/10.1016/j.gca.2008.08.017>
- Ruzicka, A., Hiyagon, H., Hutson, M., & Floss, C. (2007). Relict olivine, chondrule recycling, and the evolution of nebular oxygen reservoirs. *Earth and Planetary Science Letters*, 257(1–2), 274–289. <https://doi.org/10.1016/j.epsl.2007.02.037>
- Sanders, I. S., & Scott, E. R. D. (2012). The origin of chondrules and chondrites: Debris from low-velocity impacts between molten planetesimals? *Meteoritics and Planetary Science*, 47(12), 2170–2192. <https://doi.org/10.1111/maps.12002>
- Schneider, J. M., Burkhardt, C., Marrocchi, Y., Brennecka, G. A., & Kleine, T. (2020). Early evolution of the solar accretion disk inferred from Cr-Ti-O isotopes in individual chondrules. *Earth and Planetary Science Letters*, 551, 116585. <https://doi.org/10.1016/j.epsl.2020.116585>
- Schrader, D. L., Connolly, H. C., Lauretta, D. S., Nagashima, K., Huss, G. R., Davidson, J., & Domanik, K. J. (2013). The formation and alteration of the Renazzo-like carbonaceous chondrites II: Linking O-isotope composition and oxidation state of chondrule olivine. *Geochimica et Cosmochimica Acta*, 101, 302–327. <https://doi.org/10.1016/j.gca.2012.09.045>
- Schrader, D. L., Connolly, H. C., Lauretta, D. S., Zega, T. J., Davidson, J., & Domanik, K. J. (2015). The formation and alteration of the Renazzo-like carbonaceous chondrites III: Toward understanding the genesis of ferromagnesian chondrules. *Meteoritics and Planetary Science*, 50(1), 15–50. <https://doi.org/10.1111/maps.12402>
- Schrader, D. L., Nagashima, K., Krot, A. N., Oglione, R. C., & Hellebrand, E. (2014). Variations in the O-isotope composition of gas during the formation of chondrules from the CR chondrites. *Geochimica et Cosmochimica Acta*, 132, 50–74. <https://doi.org/10.1016/j.gca.2014.01.034>
- Schrader, D. L., Nagashima, K., Waitukaitis, S. R., Davidson, J., McCoy, T. J., Connolly, H. C., & Lauretta, D. S. (2018). The retention of dust in protoplanetary disks: Evidence from agglomeratic olivine chondrules from the outer Solar System. *Geochimica et Cosmochimica Acta*, 223, 405–421. <https://doi.org/10.1016/j.gca.2017.12.014>
- Tenner, T. J., Nakashima, D., Ushikubo, T., Kita, N. T., & Weisberg, M. K. (2015). Oxygen isotope ratios of FeO-poor chondrules in CR3 chondrites: Influence of dust enrichment and H₂O during chondrule formation. *Geochimica et Cosmochimica Acta*, 148, 228–250. <https://doi.org/10.1016/j.gca.2014.09.025>
- Tenner, T. J., Nakashima, D., Ushikubo, T., Tomioka, N., Kimura, M., Weisberg, M. K., & Kita, N. T. (2019). Extended chondrule formation intervals in distinct physicochemical environments: Evidence from Al-Mg isotope systematics of CR chondrite chondrules

- with unaltered plagioclase. *Geochimica et Cosmochimica Acta*, 260, 133–160. <https://doi.org/10.1016/j.gca.2019.06.023>
- Tenner, T. J., Ushikubo, T., Kurahashi, E., Kita, N. T., & Nagahara, H. (2013). Oxygen isotope systematics of chondrule phenocrysts from the CO3.0 chondrite Yamato 81020: Evidence for two distinct oxygen isotope reservoirs. *Geochimica et Cosmochimica Acta*, 102, 226–245. <https://doi.org/10.1016/j.gca.2012.10.034>
- Tenner, T. J., Ushikubo, T., Nakashima, D., Schrader, D. L., Weisberg, M. K., Kimura, M., & Kita, N. T. (2018). Oxygen Isotope Characteristics of Chondrules from Recent Studies by Secondary Ion Mass Spectrometry. In *Chondrules: Records of Protoplanetary Disk Processes*. Cambridge University Press, pp. 196–246. <https://doi.org/10.1017/9781108284073.008>
- Ushikubo, T., & Kimura, M. (2020). Oxygen-isotope systematics of chondrules and olivine fragments from Tagish Lake C2 chondrite: Implications of chondrule-forming regions in protoplanetary disk. In *Geochimica et Cosmochimica Acta*. The Author(s). <https://doi.org/10.1016/j.gca.2020.11.003>
- Ushikubo, T., Kimura, M., Kita, N. T., & Valley, J. W. (2012). Primordial oxygen isotope reservoirs of the solar nebula recorded in chondrules in Acfer 094 carbonaceous chondrite. *Geochimica et Cosmochimica Acta*, 90, 242–264. <https://doi.org/10.1016/j.gca.2012.05.010>
- Villeneuve, J., Chaussidon, M., Marrocchi, Y., Deng, Z., & Watson, E. B. (2019). High-precision in situ silicon isotopic analyses by multi-collector secondary ion mass spectrometry in olivine and low-calcium pyroxene. *Rapid Communications in Mass Spectrometry*, 33(20), 1589–1597. <https://doi.org/10.1002/rcm.8508>
- Villeneuve, J., Libourel, G., & Soulié, C. (2015). Relationships between type I and type II chondrules: Implications on chondrule formation processes. *Geochimica et Cosmochimica Acta*, 160, 277–305. <https://doi.org/10.1016/j.gca.2015.03.033>
- Villeneuve, J., Marrocchi, Y., & Jacquet, E. (2020). Silicon isotopic compositions of chondrule silicates in carbonaceous chondrites and the formation of primordial solids in the accretion disk. *Earth and Planetary Science Letters*, 542, 116318. <https://doi.org/10.1016/j.epsl.2020.116318>
- Wasson, J. T., Krot, A. N., Lee, M. S., & Rubin, A. E. (1995). Compound chondrules. *Geochimica et Cosmochimica Acta*, 59(9), 1847–1869. [https://doi.org/10.1016/0016-7037\(95\)00087-G](https://doi.org/10.1016/0016-7037(95)00087-G)
- Wasson, J. T., & Rubin, A. E. (2003). Ubiquitous low-FeO relict grains in type II chondrules and limited overgrowths on phenocrysts following the final melting event. *Geochimica et Cosmochimica Acta*, 67(12), 2239–2250. [https://doi.org/10.1016/S0016-7037\(03\)00023-1](https://doi.org/10.1016/S0016-7037(03)00023-1)
- Yurimoto, H., & Wasson, J. T. (2002). Extremely rapid cooling of a carbonaceous-chondrite chondrule containing very ¹⁶O-rich olivine and a ²⁶Mg-excess. *Geochimica et Cosmochimica Acta*, 66(24), 4355–4363. [https://doi.org/10.1016/S0016-7037\(02\)01218-8](https://doi.org/10.1016/S0016-7037(02)01218-8)